Check for updates

JGR Space Physics

RESEARCH ARTICLE
10.1029/2023JA032189

Constraining the Influence of Callisto's Perturbed Electromagnetic Environment on Energetic Particle Observations

Lucas Liuzzo[1], Andrew R. Poppe[1], Quentin Nénon[2], Sven Simon[3,4], and Peter Addison[3]

[1]Space Sciences Laboratory, University of California, Berkeley, Berkeley, CA, USA, [2]Institut de Recherche en Astrophysique et Planétéologie, CNRS-Université Toulouse III-CNES, Toulouse, France, [3]School of Earth and Atmospheric Sciences, Georgia Institute of Technology, Atlanta, GA, USA, [4]School of Physics, Georgia Institute of Technology, Atlanta, GA, USA

Key Points:

- We compare energetic charged particle data with a model to explain pitch angle distributions observed during four Galileo flybys of Callisto
- Electron flux drop-outs are shaped by the perturbed fields associated with Callisto's induced field and magnetospheric plasma interaction
- Observed ion fluxes can be mainly explained through geometric considerations, with Callisto's surface shadowing particles from detection

Supporting Information:

Supporting Information may be found in the online version of this article.

Correspondence to:

L. Liuzzo,
liuzzo@berkeley.edu

Citation:

Liuzzo, L., Poppe, A. R., Nénon, Q., Simon, S., & Addison, P. (2024). Constraining the influence of Callisto's perturbed electromagnetic environment on energetic particle observations. *Journal of Geophysical Research: Space Physics*, *129*, e2023JA032189. https://doi.org/10.1029/2023JA032189

Received 16 OCT 2023
Accepted 8 FEB 2024

© 2024. The Authors.
This is an open access article under the terms of the Creative Commons Attribution License, which permits use, distribution and reproduction in any medium, provided the original work is properly cited.

Abstract

This study focuses on constraining the role that Callisto's perturbed electromagnetic environment had on energetic charged particle signatures observed during the Galileo mission. To do so, we compare data from the Energetic Particle Detector (EPD) obtained during four close encounters of the moon with a model framework that combines hybrid simulations for low-energy plasma and test-particle tracing simulations for high-energy particles. By comparing model results for energetic particle dynamics in both uniform and perturbed electromagnetic fields, we systematically disentangle the role that geometric effects (i.e., absorption of particles by Callisto's solid surface) have on observed energetic particle signatures compared to those associated with Callisto's perturbed electromagnetic environment (generated by the moon's induced magnetic field and plasma interaction currents). We show that observed flux drop-outs in the energetic ion pitch angle distributions (PADs) are largely driven by their absorption by Callisto's surface: their large gyroradii exceed the size of the moon, facilitating their impact onto the icy surface and preventing their detection by EPD. However, features observed in the energetic electron PADs can only be explained with an accurate representation of the moon's perturbed environment, since electrons closely follow the orientation of the electromagnetic fields. Our findings therefore illustrate the key role that the moon's induced field and magnetospheric plasma interaction have on the dynamics of energetic electrons, emphasizing the importance of accurately modeling Callisto's locally perturbed electromagnetic environment when attempting to interpret data from past and future encounters, including those anticipated from the upcoming JUICE mission.

Plain Language Summary

Jupiter's moon Callisto is continuously exposed to a combination of low-energy plasma and high-energy charged particles. As the moon interacts with these populations, its local electromagnetic field environment becomes highly perturbed. During four Callisto encounters during the Galileo mission to Jupiter, a sensor onboard the spacecraft detected clear signatures of the high-energy ions and electrons. To understand the degree to which Callisto's low-energy plasma interaction affects these signatures, we systematically model the dynamics of energetic particles as they travel through various electromagnetic field configurations. We find that the energetic ion observations are not strongly affected by the perturbed fields, but instead can be understood in terms of the particles being absorbed by Callisto's solid surface. However, electrons are highly sensitive to the draped fields, and the Galileo observations can only be understood when considering the perturbed electromagnetic environment near the moon. Our results underscore the importance of accurately modeling Callisto's perturbed environment when hoping to understand energetic particle signatures observed during the upcoming JUICE mission.

1. Introduction

The second-largest moon in the Jovian system, Callisto (radius R_C = 2,410 km), orbits its parent planet at a distance of approximately 26.3R_J (radius of Jupiter R_J = 71,492 km). While the moon completes an orbit in approximately 16 days, the rapid rotation period of Jupiter causes Callisto to experience a synodic period every ∼10 hr. Compared to the three other Galilean moons, Callisto's magnetospheric environment is highly variable, experiencing the largest range of M-shell—defined as the jovicentric radial distance at the magnetic equator of a field line that threads the moon normalized to 1R_J—throughout its orbit, from $26.3 \lesssim M \lesssim 80$ (Liuzzo et al., 2019a; Paranicas et al., 2018). As such, the magnitude of the magnetospheric field and the ambient plasma number density near Callisto vary by approximately an order of magnitude during the moon's orbit, driven by the ∼10°

21699402, 2024, 2, Downloaded from https://agupubs.onlinelibrary.wiley.com/doi/10.1029/2023JA032189 by Univ of California Lawrence Berkeley National Lab, Wiley Online Library on [23/02/2024]. See the Terms and Conditions (https://onlinelibrary.wiley.com/terms-and-conditions) on Wiley Online Library for rules of use; OA articles are governed by the applicable Creative Commons License

tilt between the Jovian spin and magnetic axes (e.g., Kivelson et al., 2004), and the magnetospheric current sheet (e.g., Khurana & Schwarzl, 2005).

The time-variability of the magnetospheric field drives currents within conducting layers at the moon. Such layers include Callisto's highly conductive ionosphere (e.g., Hartkorn & Saur, 2017; Kliore et al., 2002) and, potentially, a salty subsurface ocean (e.g., Khurana et al., 1998; Kivelson et al., 1999; Vance et al., 2021). Currents generated within these layers manifest outside of the moon as a time-variable, induced magnetic field (see Cochrane et al., 2022; Saur et al., 2010; Zimmer et al., 2000). However, the induced field is, at different levels of intensity, obscured by additional currents generated by Callisto's interaction with its ambient magnetospheric environment: since Callisto's orbital velocity is much slower than the velocity of the (partially) corotating ambient plasma, the moon is continuously overtaken by magnetospheric ions and electrons. The magnetospheric field, frozen-in to this (partially) corotating, low-energy plasma, piles up at Callisto's orbital trailing, ramside hemisphere and drapes around the moon's flanks, potentially obscuring or even mimicking any signature of the induced field (Liuzzo et al., 2016, 2018). In addition, particles from the moon's ionosphere are picked-up and drift downstream, generating strong flow shears between the magnetospheric and ionospheric plasma populations. Due to the variability of the Jovian magnetosphere near Callisto's orbital position, the "strength" of the resulting plasma interaction is likewise variable. Hence, when Callisto is located near the center of the Jovian plasma sheet (where the magnetospheric field is weakest and the plasma number density is largest), the moon's plasma interaction dominates the magnetic perturbations. However far from the sheet (where the ambient field is strongest and the plasma density is lowest), the induced field dominates the perturbations (see, e.g., Figure 1 of Liuzzo et al., 2015).

Besides the low-energy magnetospheric plasma, Callisto is also bombarded by charged particles at higher energies. These electrons and ions (predominantly protons, oxygen, and sulfur; see, e.g., Mauk et al., 2004) extend from energies of $E \approx 10$ keV and can exceed tens of MeV (Divine & Garrett, 1983). The intensity of the energetic population likewise varies by approximately an order of magnitude over a Jovian synodic period (Liuzzo et al., 2022), and the resulting flux of particles that precipitate onto Callisto display a similar level of variability. These particles penetrate the atmosphere are responsible for weathering the moon's icy surface (e.g., Hendrix & Johnson, 2008) and help generate its atmosphere (Carberry Mogan et al., 2023).

2. Galileo at Callisto

During the primary phase of its mission, the Galileo spacecraft performed three flybys of Callisto: C3, C9, and C10. Using magnetometer measurements from the C3 and C9 encounters, multiple studies have focused on constraining Callisto's inductive response (e.g., Khurana et al., 1998; Kivelson et al., 1999; Zimmer et al., 2000). Because Callisto was located far from the Jovian magnetic equator during these first two encounters (and hence, far from the densest part of the magnetospheric plasma sheet), the plasma currents generated by Callisto's interaction with its ambient magnetospheric environment were weak during C3 and C9 (see also, Lindkvist et al., 2015; Liuzzo et al., 2015). As a result, the magnetic field perturbations detected by Galileo during these encounters could be explained largely by the superposition of the Jovian magnetospheric background field with an induced dipole field. The earliest studies using data from these two Galileo encounters (Khurana et al., 1998; Kivelson et al., 1999; Zimmer et al., 2000) therefore interpreted the magnetometer signatures as evidence for a global, subsurface ocean at Callisto, within which currents would be generated by the time-variable Jovian magnetospheric field. However, reanalysis of the magnetic field data from these encounters by Hartkorn and Saur (2017) has indicated that the magnetometer signatures from C3 (and possibly also C9) could likewise indicate induction within Callisto's ionosphere alone; that is, *without* any subsurface ocean (see also Cochrane et al., 2022; Vance et al., 2021).

The magnetic field signatures obtained during the subsequent encounter, C10, show similar signatures of an induced magnetic field near closest approach (C/A) of Callisto. Liuzzo et al. (2016) applied a hybrid (kinetic ions, fluid electrons) model to investigate the magnetic field and low-energy plasma signatures observed during this flyby and found that within the wake near the moon's surface, a quasi-dipolar "core region"—where the local magnetic field perturbations are well-explained by an induced field—was detected by the Galileo magnetometer. However, Callisto was located closer to the center of the Jovian plasma sheet during C10 than it was during C3 or C9. Hence, in contrast to these earlier encounters, the currents generated by Callisto's low-energy plasma interaction were strong: the magnetic field data inbound and outbound of C/A when far outside of the moon's geometric plasma shadow (defined in CphiO coordinates as $x > 0$, $\sqrt{y^2 + z^2} \leq R_C$, where x is along the direction of

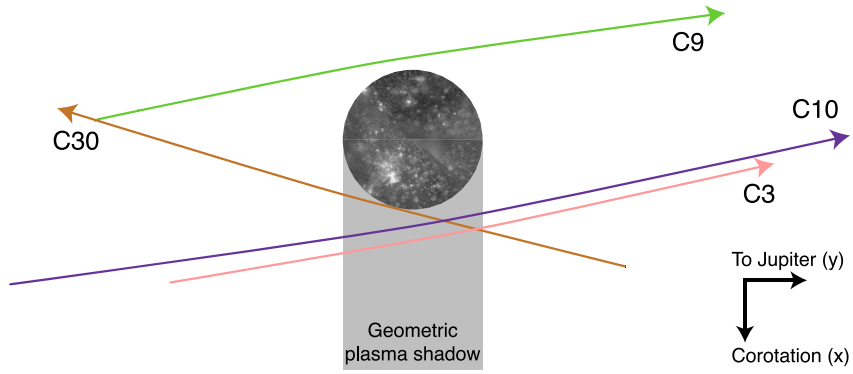

Figure 1. Trajectories of the Galileo (pink) C3, (green) C9, (purple) C10, and (orange) C30 encounters of Callisto, for which there is high-time-resolution EPD data available. The figure is from a vantage point located above Callisto's north pole, with the direction of corotation (*x* in CphiO) pointing downward along the figure's vertical axis, and Jupiter directed to the right (aligned with CphiO *y*). The nominal location of Callisto's geometric plasma shadow is represented by the shaded region, assuming the upstream flow to be aligned with the corotation direction. The figure is to scale. The mosaic of Callisto has been obtained from the United States Geological Survey (USGS, 2002).

Callisto's orbital motion, *y* points toward Jupiter, and *z* is northward completing the right-handed system; see also Figure 1) were not well-explained by the superposition of an induced field and the Jovian background field. Instead, Liuzzo et al. (2016) illustrated that the magnetic field signatures show clear indications of the magnetospheric field draping around Callisto that forms Alfvén wings at greater distances to the moon during the C10 encounter. In addition, these authors identified a rotational discontinuity in the magnetic field when Galileo passed between these two separate regions.

After Galileo's prime mission ended in 1997, the probe performed five additional close encounters of the moon (C20, C21, C22, C23, and C30). The only study to investigate the magnetic field signatures associated with Callisto's interaction during these flybys is from Liuzzo et al. (2017). These authors found that there were no signatures associated with an induced field observed at the moon during these encounters, due to strong currents associated with the variability of the ambient magnetospheric plasma during C21, a large C/A altitude during C22, and a weak inducing field during C23 and C30 (note that there is no magnetometer data from C20).

Despite these previous studies that have focused on magnetic field data from Galileo to constrain the moon's interaction with the low-energy Jovian magnetospheric plasma, there is a dearth of constraints regarding the *energetic* charged particles' interaction with the moon as observed during the Galileo encounters. Galileo's Energetic Particle Detector (EPD; Williams et al., 1992a) measured the composition of Jovian magnetospheric particles within the energy range of tens of keV up to a few MeV. EPD obtained high-resolution ("record-mode") data during four of the Callisto encounters: C3, C9, C10, and C30 (see Figure 1). Our present study will focus on "channelized" data from these four targeted encounters (see further discussion in Kollmann et al., 2022), which separates electrons and ions (protons, oxygen, sulfur) into individual energy channels. Since the other flybys (C20, C21, C22, and C23) did not collect high-resolution EPD data, we exclude these encounters from this analysis. Table 1 provides the EPD channels and their respective energy ranges that are relevant for this study. EPD was mounted on a platform with a motor that stepped over 8 positions which, when combined with a full spacecraft spin (~20 s), allowed for a nearly 4π sr field of view (FOV) for the instrument (see Appendix A and Williams et al., 1992b).

Mauk and Saur (2007) were the first to analyze data from the close Callisto encounters for which there is high-time-resolution EPD data available. These authors focused on energetic electron data to constrain their pitch angle distributions and presented a technique to characterize the "beam-ness" (i.e., how strongly these particles were aligned with the ambient magnetic field) of the observed distribution. For Galileo's closest approach of Callisto during the C3 and C9 flybys, these authors found that EPD detected highly field-aligned electron beams. Importantly, these beams seem to occur both upstream (as seen during C9) as well as downstream (detected during C3) of the moon. Recently, Nénon et al. (2022) used EPD to identify the presence of a "scattered" beam distribution of electrons at even higher energies $E \gtrsim 1$ MeV within Callisto's wake during the C3 and C30 Galileo

21699402, 2024, 2, Downloaded from https://agupubs.onlinelibrary.wiley.com/doi/10.1029/2023JA032189 by Univ of California Lawrence Berkeley National Lab, Wiley Online Library on [23/02/2024]. See the Terms and Conditions (https://onlinelibrary.wiley.com/terms-and-conditions) on Wiley Online Library for rules of use; OA articles are governed by the applicable Creative Commons License

21699402, 2024, 2, Downloaded from https://agupubs.onlinelibrary.wiley.com/doi/10.1029/2023JA032189 by Univ of California Lawrence Berkeley National Lab, Wiley Online Library on [23/02/2024]. See the Terms and Conditions (https://onlinelibrary.wiley.com/terms-and-conditions) on Wiley Online Library for rules of use; OA articles are governed by the applicable Creative Commons License

Table 1
Galileo EPD Parameters for the Channels Used in This Study as Relevant for the C3, C9, C10, and C30 Galileo Encounters of Callisto ("e" = Electrons, "i" = All Ions, "H" = Protons Only)

Channel	Species	Energy (keV)
E0	e	15–29
E1	e	29–42
E2	e	42–55
E3	e	55–93
F0	e	93–188
F1	e	174–304
F2	e	304–527
F3	e	527–884
A0[a]	i	22–42
A1	i	42–65
A2	i	65–120
A3	i	120–280
A4	i	280–515
A5	i	515–825
A6	i	825–1,680
A7	i	1,680–3,200
A8[a]	i	3,480–8,200
TP1[a]	H	80–220
TP2[a]	H	220–650
TP3[a]	H	540–785

[a]Due to instrument degradation over the mission's duration (see, e.g., Lee-Payne et al., 2020), these channels' responses (e.g., energy range, geometric factor, etc.) were different for the C30 encounter than reported here; see Kollmann et al. (2022) for further information.

encounters. While such electron beams, especially those detected within the wake, may be a signature of Callisto's interaction, Mauk and Saur (2007) emphasize the importance of separating Callisto's local environment from the broader Jovian magnetospheric environment, especially considering that the moon acts as an obstacle to the magnetospheric plasma flow and strongly perturbs the local electromagnetic fields. Previous studies were therefore unable to determine whether these energetic electron signatures were associated with the moon's local plasma interaction, or rather if they would have been generated "irrespective of Callisto's presence," especially since Galileo detected similar signatures even far from the moon (see the discussion of the C9 encounter in Mauk & Saur, 2007). Alternatively, the beams could have been created at some point along the Callisto-Jupiter circuit, within the "far-field" region at higher Jovian latitudes, whereby Alfvén waves generated by Callisto's interaction may accelerate electrons near Jupiter's polar atmosphere, as recently identified by Szalay et al. (2020) for Io and Rabia et al. (2023) for Europa. Krupp et al. (2023) have also presented EPD data from the C3, C9, C10, and C30 Galileo encounters of Callisto, and confirmed the existence of field-aligned electron beams during C3. However, none of these aforementioned studies have attempted to quantitatively constrain the influence that Callisto's perturbed environment had on the energetic particles observed by EPD during the close Galileo encounters.

Besides the aforementioned studies, Liuzzo et al. (2019a) and Liuzzo et al. (2019b, 2022) have modeled Callisto's perturbed electromagnetic environment—as generated by its induced magnetic field and the moon's interaction with its ambient low-energy plasma environment—and found a distinct influence of the draped fields on the dynamics of energetic ions and electrons as they precipitate onto the moon. For electrons in particular, while the plasma interaction reduces the globally averaged incident flux compared to a (hypothetical) case with uniform fields, it allows electrons to precipitate onto regions that cannot be accessed when the fields are uniform. For example, Figure 5 of Liuzzo et al. (2022) displays the trajectory of an electron that "swims toward upstream" within a region of reduced magnetic field magnitude located near Callisto's downstream equatorial region before precipitating onto the moon's wakeside (i.e., leading) hemisphere. Although energetic ion dynamics display a weaker dependence on the perturbed fields (due to their gyroradii r_g potentially reaching $r_g \gg R_C$), they dominate the globally averaged energy flux deposited onto the top of the moon's atmosphere by a factor of ∼3 compared to energetic electrons. The goal of these previous studies was to understand how the distribution patterns of energetic particle precipitation onto the top of the moon's atmosphere can be affected by Callisto's perturbed environment. As such, they did not analyze the energetic particle signatures observed by the EPD along any of the Galileo encounter trajectories. In addition, although Liuzzo et al. (2019a) postulated a relationship between EPD electron counts from the E0 channel obtained during the C10 encounter and Callisto's plasma interaction (see their Figure 14), these authors did not investigate such a connection in detail.

Of the previous studies that have presented EPD data obtained near Callisto (Krupp et al., 2023; Liuzzo et al., 2019a; Mauk & Saur, 2007; Nénon et al., 2022), none have modeled or constrained how the moon's plasma interaction affects the energetic particle signatures as observed by Galileo. Importantly, there has been no attempt to quantitatively constrain the effect that Callisto and its perturbed electromagnetic environment have on the energetic ions and electrons detected during close spacecraft flybys, as has been done for other outer planet moons (e.g., Huybrighs et al., 2023; Krupp et al., 2020; Poppe et al., 2018; Selesnick & Cohen, 2009). Therefore, the goal of this study is to identify the role that Callisto has in shaping energetic particle signatures detected during close spacecraft flybys. Not only is this work critical for interpreting EPD data obtained by the Galileo mission, but it will be invaluable for understanding observations during future flybys of the moon as planned for the upcoming JUpiter ICy moons Explorer (JUICE) mission.

21699402, 2024, 2, Downloaded from https://agupubs.onlinelibrary.wiley.com/doi/10.1029/2023JA032189 by Univ of California Lawrence Berkeley National Lab, Wiley Online Library on [23/02/2024]. See the Terms and Conditions (https://onlinelibrary.wiley.com/terms-and-conditions) on Wiley Online Library for rules of use; OA articles are governed by the applicable Creative Commons License

3. Modeling Callisto's Magnetospheric Environment

3.1. Callisto's Thermal Plasma Interaction

To represent Callisto's draped electromagnetic environment, we apply the *Adaptive Ion-Kinetic*, *Electron-Fluid* model (AIKEF; Müller et al., 2011), which treats ions as individual (macro)particles and electrons as a massless, charge-neutralizing fluid. Such a technique of solving the equations of motion for ions is required when modeling the local electromagnetic field perturbations associated with Callisto's plasma interaction, since ion gyroradii near the moon can exceed $10R_C$. Indeed, the asymmetries associated with ion gyration have been well documented to be a key aspect of Callisto's perturbed electromagnetic environment (e.g., Kivelson et al., 2004; Liuzzo et al., 2015, 2016, 2017, 2018; Lindkvist et al., 2015), for which a fluid treatment of the ions would be invalid.

To help interpret the energetic particle signatures observed during the Galileo encounters, we apply the results from previous modeling studies of Callisto's electromagnetic field environment. For C3 and C9, we use the AIKEF output published by Liuzzo et al. (2015). Although these authors did not include the effect of Callisto's atmosphere/ionosphere on the local magnetic field perturbations observed along the C3 and C9 trajectories, they found that the B_x and B_y signatures agreed well with the (weak) interaction between a magnetic field induced at Callisto and the ambient magnetospheric plasma (see also, e.g., Hartkorn & Saur, 2017; Kivelson et al., 1999; Lindkvist et al., 2015). For C10, we use the AIKEF model results from Liuzzo et al. (2016), who showed that the Galileo magnetometer detected clear signatures of plasma interaction *and* induction near the moon. For C30, there are no studies that have modeled Callisto's interaction to understand the observed electromagnetic signatures. This is, in part, due to the small C/A altitude of ∼130 km ($0.05R_C$) during the encounter, as well as a crossing of the Jovian current sheet associated with a reversal in sign of the B_y component, each of which make C30 difficult to model. While Liuzzo et al. (2017) compared the perturbations associated with a dipole field induced within Callisto's interior to the magnetometer data obtained along the C30 trajectory, they only found limited agreement between the data and this analytical approach. Hence, while we can constrain the role of Callisto's draped environment on EPD data from the C3, C9, and C10 encounters, we can only provide a cursory investigation of how the solid body of the moon itself would have affected signatures detected during C30. Regardless, this is an important first step for future studies that may wish to focus on C30 observations to, for example, separate the signatures of energetic magnetospheric particle precipitation from those associated with the moon's interaction with the low-energy plasma (as discussed in Mauk & Saur, 2007; Nénon et al., 2022).

Properties of the AIKEF hybrid model in general, and details on Callisto's electromagnetic environment during these four Galileo encounters in particular, can be found in Liuzzo et al. (2015) and Liuzzo et al. (2016, 2017). We therefore refrain from providing an additional discussion of the specifics herein, and instead point the reader to the aforementioned publications for further details.

3.2. Callisto's Energetic Particle Environment

To understand the Galileo EPD observations, we use the *Galilean Energetics Tracing model* (GENTOo; Liuzzo et al., 2019a, 2019b, 2022). This model applies the output of AIKEF to trace energetic particles through Callisto's perturbed electromagnetic environment, and calculates the flux associated with those particles as they precipitate onto the moon. GENTOo is a backtracing approach that applies Liouville's theorem to convert the flux of particles in the ambient plasma into near-surface fluxes, and therefore does not consider the role of particle scattering or energy loss as it travels through Callisto's atmosphere. However, Carberry Mogan et al. (2023) has illustrated that electrons and ions above energies of 1 and 10 keV, respectively, lose a negligible amount of energy as they pass through the atmosphere since their collision cross sections shrink with increasing energy (see also Haynes et al., 2023). These energies are nearly an order of magnitude *lower* than the lowest-energy channels of the EPD instrument (which could detect electrons as low as 15 keV and protons as low as 80 keV), so we consider the role of collisions for particles at energies observable by EPD negligible for this study. Additionally, Haynes et al. (2023) have shown that charge exchange between the incident magnetospheric ions and Callisto's neutral atmosphere generates energetic neutral atoms near the moon. Furthermore, Huybrighs et al. (2020) found that, for one low-altitude flyby of Europa, particle tracing simulations of energetic protons including atmospheric charge exchange show slightly better agreement with EPD observations than simulations without it. However, for more distant encounters, Huybrighs et al. (2023) have shown that atmospheric charge exchange only subtly affected the EPD proton measurements near Europa. Similarly, Addison et al. (2021) have found that charge exchange only plays a minor role in shaping the energetic particle precipitation patterns and fluxes near Europa. Since we do not

include these effects within our modeling framework, their role in shaping the EPD signatures near Callisto is an uncertainty in our approach.

To compare the Galileo observations with our modeled results, we focus on the particles' pitch angle distributions (PADs). During close moon encounters, EPD observed all pitch angles over the course of a full sweep of the motor stepper from its lowest setting (often motor position 0) to its highest setting (often position 7; see discussion in Appendix A and Figure A1 for further information). Hence, to ensure the maximum coverage for the range of pitch angles α that can be observed, we average the EPD measurements in each energy bin over a full sweep of the instrument stepper motor for all plots displaying pitch angle distributions. For each of these encounters, one full sweep of the stepper motor was completed in ∼2 min. Since the gyroperiods of the energetic particles are well below this time, such an integration does not introduce any bias into our analysis. In general, we bin the EPD pitch angles into 10° increments, but in certain cases we increase this size to 20° in order to improve the signal-to-noise ratio. Note that we do not consider ion or electron data from motor position 0, the counts from which are altered by the instrument's background shield (see Kollmann et al., 2022). In addition, we exclude data obtained from motor position 7 for the ions, which has been shown to be associated with a periodic signature of artificially reduced fluxes during certain spins (Jia et al., 2021). Note that for the Callisto encounters studied herein, the electron counts do not show any sign of artificial drops when the EPD motor was at position 7. As further confirmation, Nénon (2022) provide time series of the raw EPD counts during these encounters, and there is no visible reduction associated with motor position 7 for electrons. We therefore conclude that whatever issue affects EPD ion measurements did *not* play a role in the electron measurements from these Callisto flybys, and we do not remove the counts obtained from motor position 7 for our analysis of electrons.

To model these particles in GENTOo, we discretize the trajectory of each Galileo encounter into ∼30 points, each corresponding to the midpoint of the window over which we average EPD observations. For every such point, we initialize particles at a single energy, corresponding to the center energy of an EPD bin (see Table 1). At each location along the trajectory, particles are initialized at an angular resolution of 0.5° in pitch angle and 1° in gyrophase. That is, the velocity vectors of the 360 particles initialized at a given pitch angle α form a cone with an opening angle of 2α, the tips of which populate a circle around the direction of the local magnetic field separated by 1° increments. We assume that the ambient particle distributions are isotropic, which is consistent with the distribution of energetic ions and electrons near Callisto's orbital distance (Mauk et al., 2004; Nénon et al., 2022). Because EPD observes a full 4π sr during one sweep of the instrument stepper motor, we initialize particles across the full sky, representing EPD's full FOV during the ∼2 min averaging window. This approach provides the advantage of not requiring information on the instantaneous look direction of the EPD instrument (corresponding to only a ∼15° FOV). Instead, this technique allows us to obtain a full-sky view of the energetic particles impinging onto the detector, and our simulation results show no strong dependence on gyrophase effects. If at any time a backtraced particle collides with Callisto's surface, its trajectory is “forbidden” and is deleted from the simulation. On the other hand, if a particle never impacts Callisto's surface and escapes the moon's local environment (potentially including multiple bounces through the magnetosphere; see Liuzzo et al., 2019a, 2022), its trajectory is “allowed” and represents a detection by EPD.

We note that the above approach makes the following assumptions. Since we only model particles at the center energy of an EPD channel, we rely on the fact that a particle's gyroradius is not too different between the lower and upper energy thresholds of the channel. If this were not the case, the dynamics of a particle at the upper end of the energy range (e.g.,) would be different from those of a particle at the center energy. In such a scenario, the model would not accurately represent the higher energy particle's trajectory or dynamics through the local environment. However, for the EPD proton and electron channels, the particles' gyroradii at the upper and lower energies remain within a factor of ∼2 of one another. We have performed additional simulations using multiple energies covered by a single bin (e.g., for the TP1 channel, from energies $E = 130$ keV to $E = 220$ keV) and have confirmed that the simulated PADs are not strongly influenced by this treatment. This holds true even for particles whose gyroradii exceed the size of Callisto (i.e., high-energy ions), since the gyroradii of particles at the energies defined by the edges of an EPD bin remain within a factor of ∼1.5 of one another. Additionally, since we average the PADs over a single motor sweep of the instrument and only run GENTOo at a single position along the trajectory for each sweep, we assume that the local magnetic field geometry does not change too much over this time frame. During its Callisto encounters, Galileo traveled approximately 8 km/s, covering less than $0.4R_C$ during each two-minute averaging window. These scales are comparable to certain magnetic field structures observed by Galileo near the moon (see, e.g., Liuzzo et al., 2016), so any features associated with energetic

21699402, 2024, 2, Downloaded from https://agupubs.onlinelibrary.wiley.com/doi/10.1029/2023JA032189 by Univ of California Lawrence Berkeley National Lab, Wiley Online Library on [23/02/2024]. See the Terms and Conditions (https://onlinelibrary.wiley.com/terms-and-conditions) on Wiley Online Library for rules of use; OA articles are governed by the applicable Creative Commons License

particles that occur over these timescales are smeared out by our analysis. However, since the most prominent signatures of Callisto in EPD data are visible in the particle pitch angle distributions (i.e., the flux spectra along the trajectory were often featureless; see Section 4 or Krupp et al., 2023), this approach maximizes coverage in pitch angle space when interpreting Galileo energetic particle data near Callisto.

4. Results

4.1. The Galileo C10 Encounter

Figure 2 displays observations obtained during the C10 encounter of Callisto, which occurred on 16–17 September 1997. Figure 2a shows data from Galileo's magnetometer, which indicates Callisto's position below the center of the Jovian magnetic equator during the flyby: the magnetospheric background field was mainly pointed toward Jupiter with a strong B_y component. As discussed in Liuzzo et al. (2016), the background field was slightly inhomogeneous during the encounter, with the magnitude of the field measured along the inbound segment of the trajectory nearly 15 nT lower than during the outbound portion (increasing from a value of $|\mathbf{B}_0| \approx 25$ nT to $|\mathbf{B}_0| \approx 40$ nT). This gradient is consistent with the magnetospheric plasma sheet sweeping over Callisto throughout the encounter: as its distance to the Jovian magnetic equator increases (i.e., the moon moves to larger magnetic latitudes), Callisto is connected to field lines from increasing M-shells corresponding to a (locally) enhanced magnetospheric field magnitude (see also, e.g., Khurana, 1997; Kivelson et al., 1999).

This behavior is also evident in the remaining panels: Figures 2b and 2c include the differential energy flux for electrons (E and F channels of EPD) and all ions (A channels of EPD), respectively, during the encounter, while Figures 2d and 2e show the pitch angle distributions (PADs) of electrons and protons from the EPD E0 (15 keV $\leq E \leq$ 29 keV) and TP1 (80 keV $\leq E \leq$ 220 keV) channels, respectively. As visible in these panels, the particle differential energy flux decreased by a factor of ∼5 at all energies throughout the encounter. As illustrated by Liuzzo et al. (2022), the ambient energetic particle fluxes near Callisto's orbit vary by approximately an order of magnitude (see their Figure 3); so, such a reduced energetic particle flux in Figure 2 is consistent with the moon traveling to successively increasing M-shells throughout the encounter.

Besides the gradual reduction in energetic particle flux displayed in Figures 2b–2e, additional signatures are visible in the EPD data. A series of drop-outs are visible in the energetic ion observations that became increasingly large as Galileo approached C/A (see Figure 2c). For the bite-outs located on either side of C/A, ions at energies $E \gtrsim 300$ keV were prevented from entering the detector, suggesting absorption by Callisto before these particles could be detected by EPD. Note that the periodic dark gray bars in Figure 2c across all ion energies correspond to measurements that have been excluded from our analysis, since they correspond to times when the EPD was at motor position 7 (resulting in an artificially reduced flux; see Jia et al., 2021). However, the broad bite-outs observed at higher energies, especially those just before and after closest approach, are *not* associated with this instrumental effect since the EPD motor was not at position 7 during these times. A similar signature was also detected for energetic electrons after C/A near 00:22 (see Figure 2b), where the flux was reduced at all energies by nearly an order of magnitude for approximately 2 min. These drop-outs occurred within Callisto's geometric plasma shadow (shaded area of Figure 2a) and were centered around a tangential discontinuity in the magnetic field detected by Galileo. Liuzzo et al. (2016) identified this feature as the sharp boundary between Callisto's induced field and sub-Jovian Alfvén wing.

The signatures visible in the particle fluxes also map into their pitch angle distributions. Figures 2d and 2e show that these features coincide with reduced particle differential fluxes centered near $\alpha \approx 90°$ for electrons in the E0 channel (center energy $E = 21$ keV) and protons in the TP1 channel (center energy $E = 133$ keV). Note that the TP1 channel shown in Figure 2e only detects protons, whereas the A channels included in Figure 2c are sensitive to all ions. Besides the drop-outs on either side of C/A, additional, short-scale depletions at ∼20s intervals in the ion energy flux (see panel 2c) correspond to times when the detector scanned through pitch angles near 90°, where ions with large gyroradii impact Callisto. In addition, the proton PAD indicates a broader trend: from approximately 00:10 UTC (before entry into the geometric plasma shadow) through 00:25 UTC (after exit of the shadow), there is a band of reduced differential energy flux that starts near 130° and extends down to pitch angles of $\alpha \approx 50°$. EPD detected similar signatures in the PADs of energetic oxygen and sulfur ions, which are not shown in the interest of brevity. This broad-scale depletion structure in the TP1 channel (ranging from pitch angles of $50° \lesssim \alpha \lesssim 130°$) corresponds to the bite-outs that are visible in Figure 2c. These features are most clearly visible before and after closest approach, but occur multiple times between 00:10 UTC and 00:30 UTC.

21699402, 2024, 2, Downloaded from https://agupubs.onlinelibrary.wiley.com/doi/10.1029/2023JA032189 by Univ of California Lawrence Berkeley National Lab, Wiley Online Library on [23/02/2024]. See the Terms and Conditions (https://onlinelibrary.wiley.com/terms-and-conditions) on Wiley Online Library for rules of use; OA articles are governed by the applicable Creative Commons License

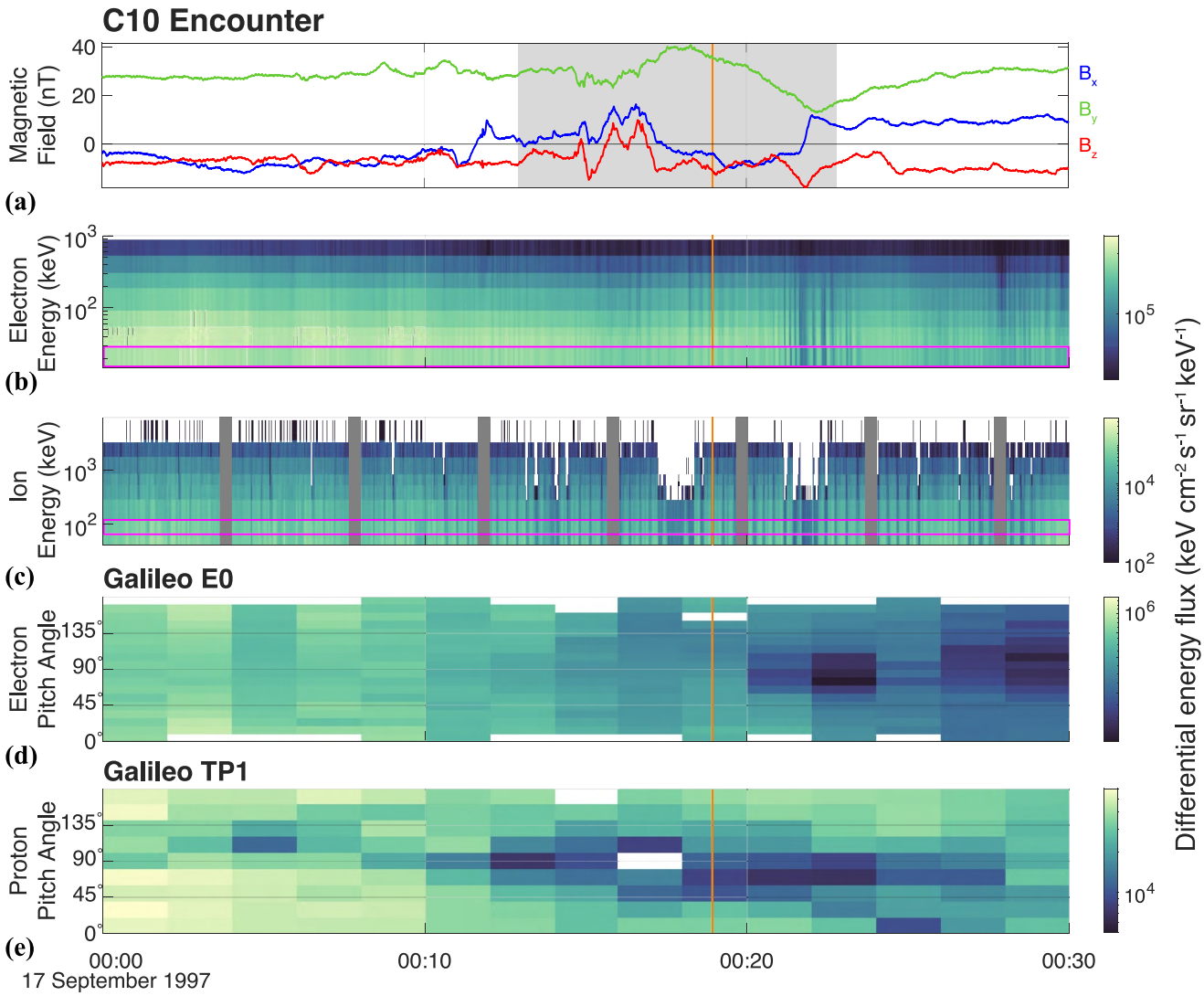

Figure 2. Galileo measurements during the C10 encounter. Panel (a) includes the magnetic field components in the CphiO system, while panels (b) and (c) include the differential energy flux of electrons (Galileo E and F channels) and all ion species (Galileo A channel), respectively. The observed PADs of (d) electrons in the E0 channel (15 keV $\leq E \leq$ 29 keV) and (e) protons in the TP1 channel (80 keV $\leq E \leq$ 220 keV) are included, averaged over a full spacecraft spin and stepper motor cycle. Pink boxes in panels (b, c) indicate the energy range observed by the EPD E0 and TP1 channels, while the vertical orange line indicates Galileo's closest approach. Gray shading in panel (a) denotes the location of Callisto's geometric plasma shadow. Note that the periodic dark gray bars occurring across all energies in panel (c) correspond to times when EPD was at motor position 7, the values of which have been removed. See text for further detail.

To further understand the features present in the PADs for energetic particles during the C10 encounter, Figure 3 compares Galileo measurements (panels a, b, e, and f) with GENTOo model results (panels c, d, g, and h). Figures 3a and 3e illustrate a projection of the Galileo C10 encounter trajectory onto the *x*-*y* plane, which is colored to the measured magnetic field magnitude. While these panels are identical, they are both included to facilitate comparison with the energetic particle signatures in each respective column since the spatial range shown for the trajectory is the same as the time range shown for the PADs. Just before closest approach (orange star in Figures 3a and 3e) and within the geometric plasma shadow (gray shading), Galileo detected a maximum in |**B**|, where the superposition of Callisto's induced magnetic field and the Jovian magnetospheric field results in an enhancement of |**B**| close to Callisto's central wake (see Figure 2a). Immediately after closest approach as the spacecraft exited the geometric plasma shadow, Galileo detected a minimum in |**B**| (see also Liuzzo et al., 2016).

Figures 3b–3d show the normalized PADs of $E \approx 21$ keV electrons, averaged over a full sweep of the EPD stepper motor, as (b) observed by Galileo and (c–d) modeled with GENTOo. For each panel, the flux is normalized to the

21699402, 2024, 2, Downloaded from https://agupubs.onlinelibrary.wiley.com/doi/10.1029/2023JA032189 by Univ of California Lawrence Berkeley National Lab, Wiley Online Library on [23/02/2024]. See the Terms and Conditions (https://onlinelibrary.wiley.com/terms-and-conditions) on Wiley Online Library for rules of use; OA articles are governed by the applicable Creative Commons License

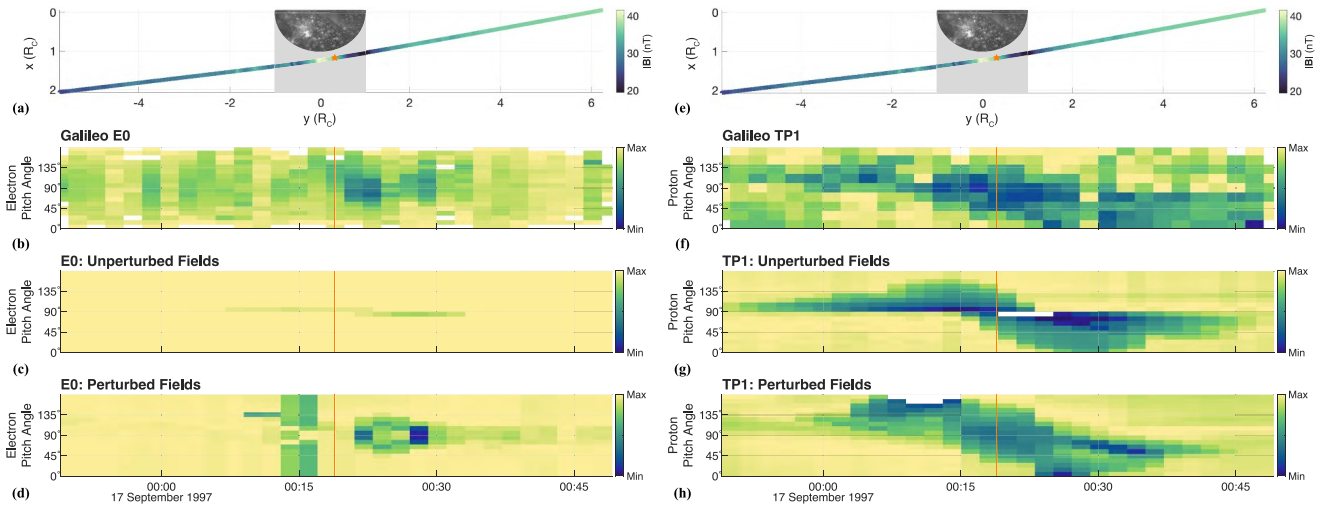

Figure 3. Pitch angle distribution of energetic (left column) electrons and (right column) protons during the C10 encounter. Panels (a, e) display the trajectory of the encounter, projected onto the CphiO *x*-*y* plane and colored corresponding to the observed magnetic field magnitude. Panels (b, f) correspond to the PADs observed in the electron E0 and ion TP1 channels of EPD, respectively, while panels (c, d) and (g, h) are from the model. The orange stars and vertical lines denote Galileo's closest approach. Pitch angles are averaged over a full sweep over the EPD stepper motor and are normalized to the maximum value detected over each sweep. See text for further detail.

maximum value detected at any pitch angle during each individual stepper motor cycle, which emphasizes changes in the differential flux across the range of possible pitch angles within a given two-minute interval. Again, note that the trajectory in Figure 3a is aligned in time with the PAD measurements given in Figures 3b–3d, and that the time range in Figure 3 is broader than in Figure 2. As was also visible in Figure 2d, the E0 EPD channel shows a clear bite-out in the electron PAD near $\alpha \approx 90°$ after closest approach, where the observed differential flux was reduced by nearly an order of magnitude compared to more field-aligned electrons. Elsewhere along the inbound and outbound portions of the trajectory, the distribution appeared mostly isotropic.

To compare to the EPD observations, Figure 3c includes GENTOo modeling results of $E = 21$ keV electrons as they travel through *unperturbed* fields (without any contributions from Callisto's interaction with its magnetospheric environment or from induction within any conducting layers). We emphasize that plasma interaction and induction signatures near the moon strongly perturb the local electromagnetic fields, but this hypothetical field configuration allows us to disentangle these physical effects from geometric considerations wherein Callisto's surface simply absorbs particles and blocks them from EPD's FOV, preventing their detection. The background magnetospheric field near Callisto was spatially inhomogeneous along the C10 trajectory (especially along the *y*-direction), so the ambient field we use for modeling energetic particle dynamics in Figure 3c was not spatially uniform near the moon. Hence, we refer to this as the "unperturbed fields" case, since it does not include any perturbations associated with Callisto's plasma interaction or inductive response (for further discussion on the background field during C10, see Liuzzo et al., 2016). Again, recall that we only model electrons at the center energy of the E0 channel ($E = 21$ keV), not the full range from 15 keV $\leq E \leq$ 29 keV.

Figure 3c illustrates that for this case of *unperturbed* fields, there are nearly no signatures in the modeled PAD. Since the gyroradius of an $E = 21$ keV electron is only $r_g \approx 0.01 R_C$ in these fields (compared to a C/A altitude of $0.22 R_C$), and since Galileo did not cross magnetic field lines that were connected to Callisto's surface during C10, the modeled electron PAD using these unperturbed fields is nearly featureless. Only a slight reduction in the particle flux is visible in Figure 3c, with a minor drop in the electron PAD at angles $\alpha \approx 90°$ caused by energetic electrons impacting Callisto's surface. Since electrons with near-perpendicular pitch angles only travel small distances along the Jovian magnetospheric field before mirroring, they return close to the moon with only a minimal displacement in the azimuthal direction associated with their net drift motion (see also Liuzzo et al., 2019a, 2022). Hence, the incident flux tubes are partially emptied of these particles before the field lines reach the location of Galileo downstream of the moon, generating this slight decrease in $\alpha \approx 90°$ electrons for this case of unperturbed electromagnetic fields visible in Figure 3c. However, while this approach provides insight into the role that absorption by Callisto's solid body has on the energetic electron PADs, unperturbed electromagnetic

21699402, 2024, 2, Downloaded from https://agupubs.onlinelibrary.wiley.com/doi/10.1029/2023JA032189 by Univ of California Lawrence Berkeley National Lab, Wiley Online Library on [23/02/2024]. See the Terms and Conditions (https://onlinelibrary.wiley.com/terms-and-conditions) on Wiley Online Library for rules of use; OA articles are governed by the applicable Creative Commons License

fields do not well-represent Callisto's environment during C10. As such, the modeled pitch angle distribution of these electrons does not agree with the EPD signatures observed during this encounter displayed in Figure 3b.

Instead, the combination of induced fields and Callisto's interaction with its plasma environment had clear effects on the magnetic field observed by Galileo (see Liuzzo et al., 2016). Figure 3d presents the result of the GENTOo model when tracing $E = 21$ keV electrons through this perturbed electromagnetic environment. The modeled electron PAD shows a region of reduced flux near values of $\alpha \approx 90°$ from 00:20 UTC until 00:40 UTC, occurring at nearly the same time as the PAD depletion observed by EPD (cf. Figure 3b). The modeled bite-out is symmetric about a pitch angle of $\alpha = 90°$ (with depletions from $40° \leq \alpha \leq 140°$) and is broad, lasting ∼10 min corresponding to an extent of nearly $1.5R_C$ along the trajectory. When compared to the case with unperturbed fields (cf. Figure 3c), it is clear that this depletion is driven by electron dynamics in the Callisto's locally perturbed electromagnetic environment; that is, these electrons are prevented from reaching this location along the Galileo trajectory. This behavior has also been characterized in Cassini measurements of energetic electrons obtained near Saturn's moon Rhea (see Roussos et al., 2012). In addition, a similar effect of the locally perturbed electromagnetic fields affecting Galileo EPD signatures has been shown for energetic *protons* near Europa (Huybrighs et al., 2023). Since the gyroradius of an $E \approx 133$ keV proton near Europa is comparable to the gyroradius of an $E \approx 21$ keV electron gyroradii near Callisto (on the order of 1% the respective moon's radius), a similar effect is visible in EPD data near each of these moons.

As visible in Figure 3a, the magnetic field was minimized within this region of reduced electron flux. Near 00:20 UTC (i.e., after C/A) and while still within Callisto's geometric plasma shadow, Galileo entered a region where the magnetic field environment was dominated by signatures of field line draping and Callisto's sub-Jovian Alfvén wing (associated with $B_x > 0$; see Figure 2a). At this time, EPD detected a bite-out in the PAD of the E0 channel for electrons with pitch angles from $50° \lesssim \alpha \lesssim 130°$. The signatures of field line draping (in magnetometer data) and the bite-out of electrons at near-perpendicular pitch angles (in EPD data) persisted through the exit of the geometric shadow until approximately 00:32 UTC, after which both sets of observations returned to their background states. When considering Callisto's perturbed environment, the modeled electron PAD in Figure 3d displays a reduced flux for electrons with $40° \lesssim \alpha \lesssim 140°$ after closest approach from 00:20 UTC–00:30 UTC, consistent with the bite-out observed by Galileo at this time. This region of reduced flux cannot be reproduced for the case with unperturbed electromagnetic fields (cf. Figure 3c) since it does not include any signatures of Alfvén wings (or field line draping). Hence, it is likely that the feature detected by EPD after C/A in the E0 channel is driven by Callisto's sub-Jovian Alfvén wing, as generated by the moon's interaction with its ambient plasma environment.

After 00:32 UTC, the model suggests a continued reduction of the electron differential flux near $\alpha \approx 90°$ through 00:45 UTC, nearly 15 min after the Galileo E0 PAD became isotropic (and the magnetic field returned to its background value). This discrepancy can be understood in terms of the modeled magnetic field within this region: as seen in Figure 3 of Liuzzo et al. (2016), the sub-Jovian Alfvén wing within the model extended approximately $2.5R_C$ further along the trajectory (i.e., lasted ∼10 min longer) than the wing observed by Galileo. As such, the modeled energetic electrons within this region still experience a perturbed magnetic environment, causing their resulting pitch angle distribution to slightly deviate from isotropic. Regardless, this analysis highlights that including an accurate representation of Callisto's perturbed electromagnetic environment during the C10 encounter allows for a more complete understanding of the observed energetic electron signatures, compared to modeling electron dynamics in unperturbed fields.

Interestingly, neither the observed nor the modeled PADs suggest a similar drop-out in electrons at near-perpendicular pitch angles *before* closest approach, despite Galileo's passage through the moon's anti-Jovian Alfvén wing from 00:05 UTC until approximately 00:15 UTC (see also Liuzzo et al., 2016). The modeled PAD even suggests an *enhanced* flux of electrons at pitch angles of $\alpha \approx 90°$ near 00:15 UTC compared to fluxes at more field-aligned angles, whereas the E0 channel detected a quasi-uniform distribution across all pitch angles at this time. Note that since Figure 3d displays fluxes that are normalized to the maximum value, this feature within the model results appears as reduced electron fluxes at $\alpha \lesssim 60°$ and $\alpha \gtrsim 120°$. At this location within the moon's geometric plasma shadow, the spacecraft traveled through a highly non-uniform region associated with a rapid enhancement in the magnetic field that lasted for ∼2 min. This feature was suggested to be magnetospheric in origin (see Liuzzo et al., 2016), and it is possible that the field fluctuations caused any bite-out signature to disappear.

21699402, 2024, 2, Downloaded from https://agupubs.onlinelibrary.wiley.com/doi/10.1029/2023JA032189 by Univ of California Lawrence Berkeley National Lab, Wiley Online Library on [23/02/2024]. See the Terms and Conditions (https://onlinelibrary.wiley.com/terms-and-conditions) on Wiley Online Library for rules of use; OA articles are governed by the applicable Creative Commons License

21699402, 2024, 2, Downloaded from https://agupubs.onlinelibrary.wiley.com/doi/10.1029/2023JA032189 by Univ of California Lawrence Berkeley National Lab, Wiley Online Library on [23/02/2024]. See the Terms and Conditions (https://onlinelibrary.wiley.com/terms-and-conditions) on Wiley Online Library for rules of use; OA articles are governed by the applicable Creative Commons License

Figures 3f–3h show the normalized PAD of $E \approx 133$ keV protons during the C10 encounter from (f) the TP1 channel of EPD, (g) modeled using unperturbed fields (i.e., no plasma interaction or induction effects), and (h) modeled using the perturbed fields from AIKEF. As is even more clear in Figure 3f than in Figure 2e, the proton PAD displays a banded pattern where the (normalized) differential flux was reduced, extending far beyond the location of Callisto's plasma wake and interaction region: along the inbound portion of the trajectory, a decrease of protons with pitch angles near $\alpha \approx 180°$ was detected, descending toward values of $\alpha \approx 90°$ near closest approach, and continuing to even lower pitch angles near $\alpha \approx 0°$ along the outbound leg of the trajectory.

Model results displayed in Figures 3g and 3h show quantitatively similar behavior as observed by Galileo, for both unperturbed and perturbed fields. Since the gyroradius of a $E = 133$ keV proton in the ambient magnetospheric field during C10 is $r_g \approx 0.6R_C$, energetic protons are less affected by smaller-scale perturbations to the field than the energetic electrons (see also Liuzzo et al., 2022). Instead, the similarity between the data and both model scenarios suggests that the reduced ion differential fluxes visible in Figures 2 and 3 can be explained largely by geometric considerations. During the C10 encounter, the magnetospheric field had a strong component along the $y > 0$ direction; that is, it was mainly pointed toward Jupiter, with an additional southward ($z < 0$) component. Along the inbound portion of the trajectory, Galileo was located in Callisto's $y < 0$ (anti-Jovian) hemisphere, as also illustrated in Figure 1. Particles with pitch angles of $\alpha < 90°$ (traveling with field-aligned velocities toward Jupiter) were therefore able to travel toward Galileo and reach EPD unencumbered by the moon. On the other hand, particles with pitch angles $\alpha > 90°$ (with anti-field-aligned velocities) traveled from Callisto's sub-Jovian hemisphere toward the spacecraft. Although Galileo did not cross a field line that was connected to Callisto (bite-outs at large, field-aligned pitch angles would have otherwise been detected), these particles with gyroradii $r_g \approx 0.6R_C$ would have impacted Callisto's southern, sub-Jovian surface before reaching the spacecraft's position located on the other (i.e., anti-Jovian) side of Callisto. Therefore, this geometric argument can explain the signature of reduced proton flux at pitch angles $\alpha \geq 90°$ observed prior to closest approach in Figures 3f–3h.

After C/A along the outbound portion of the trajectory, flux drop-outs in the proton PAD gradually shifted to lower pitch angles: the flux of $E \approx 133$ keV protons with $\alpha \leq 90°$ was reduced, while the flux at larger pitch angles $\alpha > 90°$ returned to a more uniform pattern. At this point along its trajectory, Galileo was located in Callisto's sub-Jovian hemisphere. Hence, particles that are located on the anti-Jovian side of Callisto but moving toward Jupiter first impact the moon's surface before they can reach the location of Galileo. That is, these protons with a velocity component parallel to the ambient magnetic field direction (i.e., with $\alpha < 90°$) gyrate into Callisto's northern, anti-Jovian surface, rendering them undetectable by EPD at Galileo's position on the other side of the moon. As such, a reduced proton flux was detected at pitch angles $\alpha \lesssim 90°$ after closest approach of the moon.

In summary, Galileo detected clear signatures of Callisto within energetic particle data during the C10 encounter. Energetic proton features were not strongly affected by Callisto's perturbed environment, but the observed drop-outs are consistent with particle shadowing by the moon's surface. Energetic electrons, on the other hand, were affected by the perturbed fields: the strongest decrease in differential flux was coincident with Galileo's crossing of Callisto's sub-Jovian Alfvén wing, which is generated by the moon's interaction with the Jovian magnetospheric plasma. Hence, it is not possible to interpret the observed electron PAD signatures without accurately representing Callisto's perturbed electromagnetic environment as detected during the C10 flyby. Although we have focused on only two EPD energy channels for two particle species here (E0 for electrons and TP1 for protons), similar features were detected at higher particle energies and for different species as well (i.e., oxygen and sulfur; see Krupp et al., 2023).

4.2. The Galileo C3 and C9 Encounters

Galileo's C3 and C9 encounters of Callisto occurred on 4 November 1996 and 25 June 1997, respectively (see also Figure 1). Figure 4 shows EPD observations during these flybys—with C3 on the left side of the figure and C9 on the right—in the same style as Figure 2. Similar to the C10 encounter, the spacecraft traveled from Callisto's anti-Jovian hemisphere into its sub-Jovian hemisphere during the flybys, with C3 located downstream of the moon and C9 upstream (see Figure 1). As was also visible during C10, there was a gradual gradient to the flux of energetic electrons (Figures 4b and 4g) and ions (Figures 4d and 4i) observed during the encounters. In contrast to C10, the fluxes gradually grew during C3 and C9. This behavior is consistent with the moon traveling to smaller magnetic latitudes and the resulting connection to *decreasing M*-shells (as also indicated by the diminishing strength of the

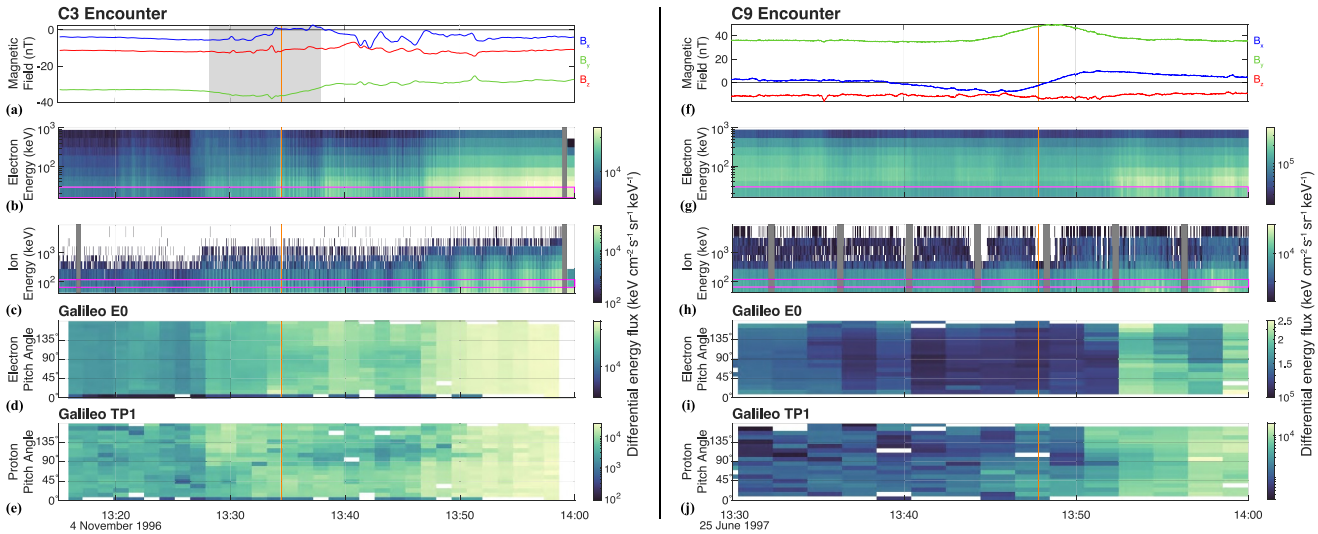

Figure 4. Galileo measurements during the (left) C3 and (right) C9 encounters of Callisto. Note the different ranges for the color scales. See Figure 2 for further detail.

magnetospheric field during the encounters; see Figure A1 of Liuzzo et al., 2015), where an enhanced energetic particle flux can be expected (Liuzzo et al., 2022).

Mauk and Saur (2007) report signatures of highly field-aligned electron distributions detected during C3, where beams at energies 15–42 keV were observed near closest approach within Callisto's wake. This feature was located near the region where Callisto's induced magnetic field was most prominent in magnetometer data (see also Figure 4a). In Figure 4d, this field-aligned electron beam is visible for $E \approx 21$ keV electrons near pitch angles of $\alpha \approx 10°$ in the bin immediately prior to closest approach. Note that the sharp reduction in the electron (and proton) energy flux near $\alpha = 0°$ is due to low count rates associated with uneven sampling of EPD at these pitch angles during the encounter. For energetic ions, the most obvious feature in the EPD observations visible in Figure 4c is in the form of a periodic pulsation to the flux of $E \lesssim 1$ MeV ions. These pulsations, characterized by changes in the differential ion energy flux by approximately an order of magnitude with a periodicity of approximately 3 min, are especially distinguishable with an increasing amplitude after ∼13:40 UTC when the spacecraft exited the moon's geometric plasma shadow. This anisotropy is the Compton-Getting effect (Compton & Getting, 1935; Gleeson & Axford, 1968), whereby the fluxes are enhanced when EPD was looking anti-parallel to (i.e., into) the corotational flow direction, and reduced when the FOV was parallel to the flow. Besides this effect, Figure 4e shows slight perturbations in the PAD of $E \approx 133$ keV protons, with a reduced flux at pitch angles of $\alpha \approx 90°$ near 13:35 UTC that expanded to pitch angles of $\alpha \lesssim 120°$ near 13:50 UTC, as was also visible during C10 (cf. Figure 2e).

In Figure 5, we compare the ion and electron PADs observed by EPD with the model results from GENTOo for the C3 flyby. As with Figure 3, the top panels (5a and 5e) show the flyby trajectory, colored to the observed magnetic field magnitude, with the orange stars indicating the location of closest approach within Callisto's geometric plasma shadow (gray shading in the panels). In the normalized electron PAD displayed in Figure 5b, the electron beams observed near Callisto (as also reported by Mauk & Saur, 2007) are evident. From just before entry into the geometric plasma shadow until closest approach (i.e., beginning near 13:24 UTC and lasting approximately 10 min), the flux of $E \approx 21$ keV electrons was maximized at pitch angles of $\alpha \approx 10°$ (see Figure 5b). This maximum indicates a beam of electrons traveling from the north of Callisto. Note that because the electron PAD displayed in panel 5b is normalized, this beam determines the value against which the fluxes of electrons at all pitch angles during this period are normalized, thereby causing an apparent *depletion* the flux in the $\alpha > 10°$ pitch angle bins, most clearly evident at closest approach. However, there is no true flux drop-out within this region. After C/A near 13:35 UTC and until 13:40 UTC (i.e., through Galileo's exit of the geometric plasma shadow), the observations indicate that this feature was flipped, with a maximum flux in electrons with pitch angles of $\alpha \approx 180°$ (i.e., populated by electrons traveling from the south of the moon). Finally, the electron signatures display a bite-out near pitch angles of $\alpha \approx 90°$ on the sub-Jovian side of Callisto near 13:45, before they returned to a nearly isotropic distribution along the outbound segment of the trajectory.

21699402, 2024, 2, Downloaded from https://agupubs.onlinelibrary.wiley.com/doi/10.1029/2023JA032189 by Univ of California Lawrence Berkeley National Lab, Wiley Online Library on [23/02/2024]. See the Terms and Conditions (https://onlinelibrary.wiley.com/terms-and-conditions) on Wiley Online Library for rules of use; OA articles are governed by the applicable Creative Commons License

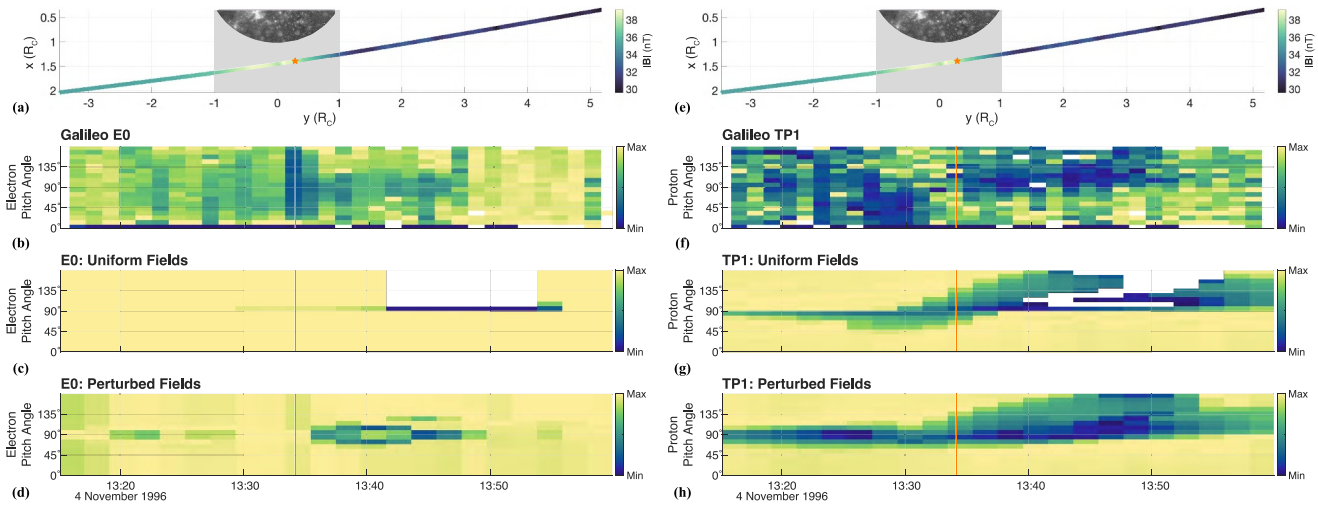

Figure 5. Normalized PADs of energetic (left column) electrons and (right column) protons during the C3 encounter. See Figure 3 and the text for further detail.

Recently, Krupp et al. (2023) have interpreted the electron PAD signatures observed along the outbound portion of the C3 trajectory to be caused by Galileo's passage through Callisto's Alfvén wing. These authors found that the region with reduced $\alpha \approx 90°$ electrons (visible in Figure 5b near 13:45 UTC) aligned well with the location of Callisto's sub-Jovian Alfvén wing tube during C3 as modeled by Seufert (2012). However, instead of applying a consistent governing system of equations to calculate the feedback between Callisto's induced field and the magnetospheric plasma interaction (see, e.g., Liuzzo et al., 2016; Neubauer, 1999), Seufert (2012) simply added a dipole magnetic field to their simulation output after it had reached a quasi-stationary state. As a result, their model overestimated the strength of the plasma interaction—and the associated electromagnetic field perturbations—for C3, and the Alfvén wing crossings suggested by their results are not reflected in the Galileo data. Indeed, numerous other studies have shown that the B_x and B_y signatures detected along the C3 encounter trajectory are well-explained by a substantially weaker plasma interaction. The electromagnetic field perturbations associated with this weak plasma interaction would therefore not be expected to deflect the energetic particles any more substantially than an induced field alone. Hence, the feature in the EPD electron data detected during C3 is likely not associated with Galileo's passage through an Alfvén wing at Callisto.

Figure 5c illustrates that a reduction in the flux of $E = 21$ keV electrons may simply be associated with particle absorption and shadowing by the solid body of the moon. For this scenario, we assume a uniform magnetic field of $\mathbf{B}_0 = (-2.4\hat{\mathbf{x}}, -31.7\hat{\mathbf{y}}, -10.8\hat{\mathbf{z}})$ nT, with $\hat{\mathbf{x}}$, $\hat{\mathbf{y}}$, and $\hat{\mathbf{z}}$ denoting unit vectors of the CphiO system. Indeed, for this (hypothetical) case, Callisto blocks *all* $E = 21$ keV electrons with pitch angles $\alpha > 90°$ from EPD's FOV between 13:39 to 13:55, corresponding to the times when the spacecraft is on (uniform) magnetic field lines connected with the moon. However, since uniform fields do not represent the electromagnetic fields near Callisto during C3, the bite-out in the modeled PAD is too broad in length, and extends to pitch angles that are too large, especially compared to the signature observed by Galileo (see Figure 5b). Indeed, the full distribution at large pitch angles of electrons with $\alpha \gtrsim 135°$ in the EPD data indicates that the spacecraft did not intersect field lines connected with Callisto.

Instead, we offer an alternative explanation for this electron bite-out near $\alpha \approx 90°$ that more accurately represents Callisto's perturbed electromagnetic environment during C3 while also considering the role that these non-uniform fields had on the EPD signatures. Figure 5d highlights that when considering the effects of Callisto's induced field and—during C3, weak—plasma interaction currents, the modeled PADs are much closer to those detected by EPD. Figure 5d illustrates that the broad region of no electron flux at $\alpha \gtrsim 90°$ in uniform fields is no longer present when including the moon's plasma interaction and inductive response. Instead, a narrow region of reduced electron flux occurs near pitch angles of $\alpha \approx 90°$, at the same time as the feature detected by Galileo. Indeed, Appendix B isolates the contribution of the induced field *alone* to these PAD signatures, and illustrates that a qualitatively similar feature can be expected when considering electron dynamics in the superposition of the magnetospheric background and induced field; that is, without the

21699402, 2024, 2, Downloaded from https://agupubs.onlinelibrary.wiley.com/doi/10.1029/2023JA032189 by Univ of California Lawrence Berkeley National Lab, Wiley Online Library on [23/02/2024]. See the Terms and Conditions (https://onlinelibrary.wiley.com/terms-and-conditions) on Wiley Online Library for rules of use; OA articles are governed by the applicable Creative Commons License

21699402, 2024, 2, Downloaded from https://agupubs.onlinelibrary.wiley.com/doi/10.1029/2023JA032189 by Univ of California Lawrence Berkeley National Lab, Wiley Online Library on [23/02/2024]. See the Terms and Conditions (https://onlinelibrary.wiley.com/terms-and-conditions) on Wiley Online Library for rules of use; OA articles are governed by the applicable Creative Commons License

effects of the moon's plasma interaction included. Hence, the decrease in electron flux detected along the outbound portion of the C3 trajectory can be primarily understood by considering the perturbed electromagnetic environment driven by Callisto's induced field and (weak) plasma interaction. Unlike the reduced electron fluxes near $\alpha \approx 90°$ that was observed during C10, the drop-out detected during C3 was not associated with particle deflection by Callisto's Alfvén wing.

An important discrepancy in the model results is a lack of strong electron beams prior to and within the geometric plasma shadow (near $\alpha \approx 10°$) and after closest approach (near $\alpha \approx 180°$) compared to the EPD observations. Although these beams could be associated with Callisto's local interaction, it is difficult to disentangle cause and effect of these beams, as discussed in Mauk and Saur (2007). While such field-aligned electron distributions were detected within the plasma shadow during C3, they were also observed along Callisto's orbital path (but far from the moon itself) during the C3 and C9 encounters where plasma interaction currents were weak. Conversely during C10, where Galileo detected clear signatures of the moon's plasma interaction in the form of field line draping (see Section 4.1 above and Liuzzo et al., 2016), the spacecraft did not observe any obvious signatures of beamed electrons. Nénon et al. (2022) note that one possible explanation for the highly field-aligned distributions of $E \gtrsim 1$ MeV electrons observed within Callisto's wake could be absorption of particles with perpendicular pitch angles by the moon's surface. Such a bite-out of electrons with pitch angles $\alpha \approx 90°$ would cause an apparent enhancement in the flux of more field-aligned electrons. However, such an interaction is unlikely to cause highly-structured, field-aligned beams, but is more likely to generate gradual pitch angle distributions (see Nénon et al., 2022). Furthermore, the lack of any broad-scale reductions extending across such a wide range of pitch angles in our model within the wake suggests that at least the observed lower-energy ($E \ll 1$ MeV) electron beams may not have been associated with the moon's interaction. Instead, they may rather be driven by larger-scale magnetospheric processes including acceleration along parallel electric fields at high Jovian latitudes (e.g., Hess et al., 2011; Knight, 1973), or even by strong potential drops near Callisto, but these effects are not captured by our model. Regardless, future observations should help to shed light on the physical mechanism responsible for generating these signatures near Callisto. Especially, measurements from the Particle Environment Package onboard JUICE will enhance our understanding of Callisto's energetic environment, since it will detect electrons and ions up to energies of 1 and 5 MeV, respectively see (Galli et al., 2022).

Additional small-scale discrepancies could be associated with differences in the observed and modeled magnetic field. While a weak interaction between the magnetospheric plasma and an induced dipole at Callisto can explain the B_x and B_y observations during C3 (e.g., Lindkvist et al., 2015; Liuzzo et al., 2015; Seufert, 2012), none of the current plasma interaction models have adequately captured perturbations detected in B_z, the component in which signatures of the moon's induced field were weakest along the C3 trajectory. Some of the largest B_z perturbations occurred near 13:45 UTC, where non-uniformities in the electron PAD were also visible (see Figure 5b and Mauk & Saur, 2007). Such signatures may be related to moon's plasma interaction or could rather be unrelated to Callisto entirely and instead be driven, for example, by waves associated with precipitating electrons (as has been detected at Rhea; see, e.g., Roussos et al., 2012; Santolík et al., 2011), or even the variability driven by magnetospheric dynamics that are omnipresent along the moon's orbit (e.g., Krupp et al., 2004).

For the energetic proton population, EPD detected a band of reduced flux after closest approach that grew in pitch angle with increasing distance to Callisto (visible in Figure 5f). Note that the recurring features at low pitch angles $\alpha \leq 10°$ with nearly no flux is associated with poor pitch angle coverage (see also the electron fluxes in Figure 5b). As was the case for C10, the model results in Figures 5g and 5h for C3 suggest that this feature can again be largely explained through geometric considerations. Inbound of Callisto, protons traveling along the field are blocked by Callisto's surface before they can reach the spacecraft, generating a flux reduction from $0° \lesssim \alpha \lesssim 90°$, although the modeled bite-out within this region does not extend to pitch angles any lower than $\alpha \approx 45°$. Note that the maxima in the normalized flux outside of this range of pitch angles therefore does not correspond to a proton enhancement or suggest the presence of any ion beams at this location (cf. Krupp et al., 2023), but is rather caused by normalization of the pitch angle distribution in the presence of regions with reduced (i.e., shadowed) particle flux. Similarly, after closest approach, the region increases to pitch angles of $90° \lesssim \alpha \lesssim 180°$, whereby protons are absorbed by the moon preventing their detection by EPD and generating the observed reduction in flux at large pitch angles. Compared to the C10

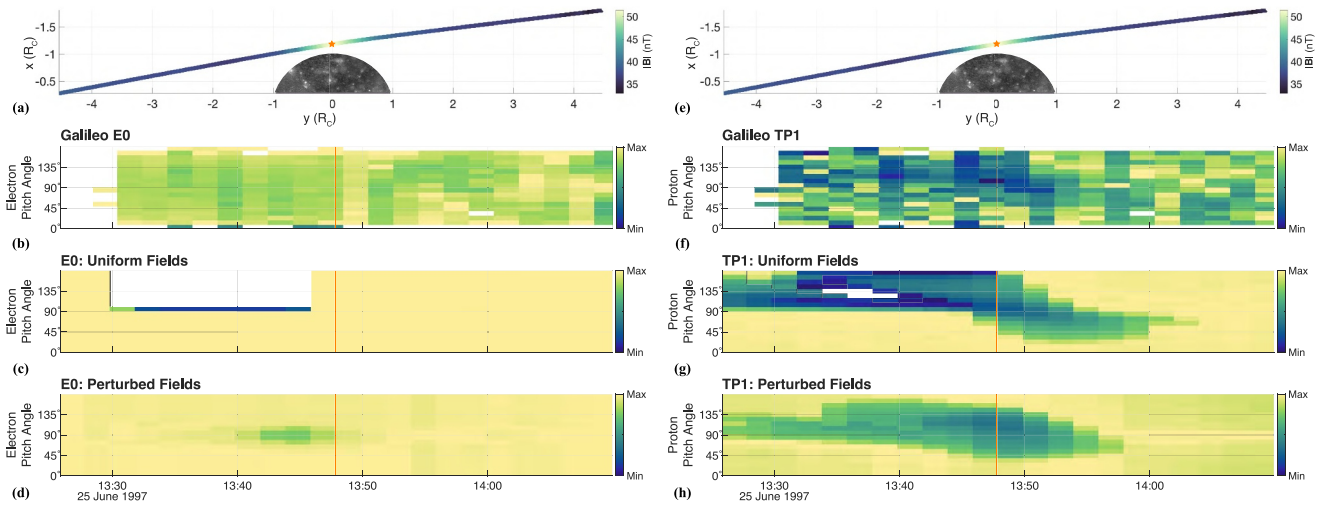

Figure 6. Normalized PADs of (left column) energetic electrons and (right column) protons during the C9 encounter. See Figure 3 and the text for further detail.

encounter, this band has been flipped with respect to a pitch angle of $\alpha = 90°$: during C3, the drop-out in field-aligned protons appeared before closest approach, while the drop-out in anti-field-aligned protons occurred after closest approach (cf. Figure 3). This difference can be understood in terms of the orientation of the background field, which had a strong component pointed *away* Jupiter during C3 (see Figure 4a), but pointed *toward* Jupiter during C10 (Figure 2a).

The C9 flyby of Galileo was the only encounter to pass through Callisto's upstream hemisphere. Since the moon was far from the center of the Jovian current sheet where the magnetospheric plasma density is low, the predominant feature in magnetometer data from the flyby was associated with an induced magnetic field at Callisto, and the superposition of the Jovian magnetospheric field with the induced field match the B_x and B_y signatures observed during this encounter (see Figure 4f or, e.g., Liuzzo et al., 2015). Besides the gradual enhancement in the flux of energetic particles throughout the encounter as visible in Figures 4g and 4h, the PAD of $E \approx 133$ keV protons depicted in Figure 4j shows distinct ion signatures of reduced flux at energies above ~700 keV before and just after closest approach. As with C3 and C10, the PAD again displays hints of a band of protons bitten-out of the distribution (see also Krupp et al., 2023). For electrons, the energy flux spectrum (Figure 4g) as well as the PAD of $E \approx 21$ keV electrons (Figure 4i) were nearly featureless and isotropic during the inbound portion of the trajectory but were slightly reduced near closest approach.

Figure 6 compares the normalized PADs of the E0 and TP1 EPD channels with modeling of $E = 21$ keV electrons and $E = 133$ keV protons during the C9 flyby. Figure 6b reveals that the electron population observed within the E0 channel were slightly field-aligned during the inbound portion of the trajectory until closest approach, with fluxes near $\alpha \approx 10°$ and $\alpha \approx 170°$ marginally enhanced compared to more perpendicular pitch angles. Mauk and Saur (2007) identified these electron beams in multiple EPD electron energy channels. This feature coincided with the region of strongest magnetic field near the moon (associated with the signature of its induced field), which likely funneled electrons traveling along the magnetospheric field lines toward this location (see also Liuzzo et al., 2019a, 2022). However, since these electron beams were also detected before and after closest approach (see Figure 6b and Mauk & Saur, 2007), it is difficult to unambiguously attribute their occurrence to Callisto and its perturbed electromagnetic environment.

For the case with uniform electromagnetic fields displayed in Figure 6b, we set $\mathbf{B}_0 = (3.3\hat{\mathbf{x}}, 33.9\hat{\mathbf{y}}, -9.4\hat{\mathbf{z}})$ nT. The complete drop-out of $E = 21$ keV electrons at pitch angles $\alpha > 90°$ from 13:30 UTC until 13:45 UTC illustrates regions where Galileo crossed field lines connected with Callisto for this for this (hypothetical) case of uniform fields. However, Figure 6b illustrates that broad feature was not observed during the encounter. The model using a more realistic representation of the local electromagnetic environment shows a much narrower reduction in the electron flux near $\alpha \approx 90°$ (Figure 6d), but elsewhere, suggests nearly isotropic electron PADs. While the model and EPD observations show reduced electron fluxes near $\alpha \approx 90°$, the EPD signatures are

21699402, 2024, 2, Downloaded from https://agupubs.onlinelibrary.wiley.com/doi/10.1029/2023JA032189 by Univ of California Lawrence Berkeley National Lab, Wiley Online Library on [23/02/2024]. See the Terms and Conditions (https://onlinelibrary.wiley.com/terms-and-conditions) on Wiley Online Library for rules of use; OA articles are governed by the applicable Creative Commons License

notably less homogeneous than the model throughout the duration of the encounter. Near closest approach, Galileo detected substantial perturbations in the B_z component of the magnetic field, which are not well-captured by the AIKEF model nor by the superposition of an induced field at Callisto with the magnetospheric background field (see also Lindkvist et al., 2015; Zimmer et al., 2000). The enhanced $|B_z|$ signature detected within this region is consistent with magnetospheric field line pileup at the moon's ramside hemisphere, which likely altered electron dynamics in a way that is not accurately represented within our model. Alternatively, it is possible that the electron beams observed within this region play a role in generating the B_z perturbations (see also discussion in Mauk & Saur, 2007). These B_z features could therefore also contribute to the discrepancy between the modeled and observed electron PADs after C/A (cf. Figures 6b and 6d). Regardless, as was also the case for C3, our results suggest that the source of these electron beams during C9 were not associated with absorption of particles with perpendicular pitch angles, and may be unrelated to Callisto's interaction with the low-energy magnetospheric plasma. However, it is beyond the scope of this study to determine how local electron dynamics are affected by, for example, potential drops at high Jovian latitudes far from the moon (e.g., Hess et al., 2011; Jacobsen et al., 2010), so we are unable to definitively identify the cause of these beams observed during C9.

For ions, Figures 6g and 6h illustrate that the broad band of reduced proton flux (beginning at large pitch angles $\alpha \approx 180°$ inbound of Callisto and extending to values of $\alpha \approx 90°$ near closest approach) is associated with shadowing by Callisto. Indeed, the gyroradius of $E = 133$ keV protons in the ambient fields approaches 75% of the moon's radius, allowing many of these particles to gyrate into Callisto's surface before their detection by EPD. Hence, as was also the case for protons during C3 and C10, the dynamics of these protons are not strongly affected by the perturbed electromagnetic environment and the reduced flux along the inbound segment can instead be explained through geometric effects. However, this band of reduced proton flux was not as well defined in the EPD observations along the outbound portion of the C9 trajectory (see Figure 6f). Instead, the distribution was more isotropic beyond 13:55 UTC, as is also suggested by the model results in uniform and perturbed fields (see Figures 6g and 6h).

4.3. The Galileo C30 Encounter

The final flyby of Callisto during the Galileo era, C30, occurred on 25 May 2001. Unlike the previous encounters, the spacecraft *approached* the moon from the sub-Jovian hemisphere, passed downstream, and *exited* the moon's environment along its anti-Jovian flank (see also Figure 1).

Figures 7a–7e show the magnetic field and energetic particle signatures from C30. The magnetospheric background field observed along the outbound and inbound portions of the Galileo trajectory was inhomogeneous: the B_y component of the magnetospheric field flipped from $B_y > 0$ before the encounter to $B_y < 0$ afterward (see Figure 7a), indicating a crossing of the Jovian current sheet (Liuzzo et al., 2017). There are many drop-outs visible in the observed electron and ion signatures in Figures 7b and 7c, some of which represent actual locations with zero counts. However, since there was poor pitch-angle coverage during the encounter—especially throughout the inbound portion of the trajectory—some of these drop-outs correspond to regions of the distribution that EPD did not detect. Others still are associated with instrumental effects where the counts are not reliable, specifically, the periodic drop-outs in the ions and electrons marked by the dark gray vertical bars in Figures 7b and 7c, corresponding to times when the EPD motor was set to position 0 (for ions and electrons) and position 7 (for ions). As such, it is difficult to separate instrumental effects from physical causes of the drop-outs seen during C30. Regardless, the spectra presented in Figure 7 show some noticeable features in the energetic particle fluxes. The high-energy electrons (above $E \gtrsim 200$ keV) display a region of reduced flux just after closest approach (Figure 7b), which coincided with a strong discontinuity in the magnetic field (Figure 7a). Liuzzo et al. (2017) suggested that this may have been associated with the dynamics of the neutral sheet between Callisto's magnetic lobes, but this feature is not clearly visible in the PAD of these electrons since the spacecraft traveled through this discontinuity on much shorter timescales than the ~2 min integration time representing a full sweep of the EPD instrument.

Galileo's closest approach to Callisto during its C30 flyby was 133 km $\approx 0.06R_C$, which is on the scale of the grid resolution of even the most advanced simulations. In addition, the Jovian magnetic equator swept over Callisto during this encounter, marked by the reversal in sign of the B_y component. For these reasons, it is not feasible to model Callisto's plasma interaction during this encounter, and we cannot study the role of Callisto's perturbed

21699402, 2024, 2, Downloaded from https://agupubs.onlinelibrary.wiley.com/doi/10.1029/2023JA032189 by Univ of California Lawrence Berkeley National Lab, Wiley Online Library on [23/02/2024]. See the Terms and Conditions (https://onlinelibrary.wiley.com/terms-and-conditions) on Wiley Online Library for rules of use; OA articles are governed by the applicable Creative Commons License

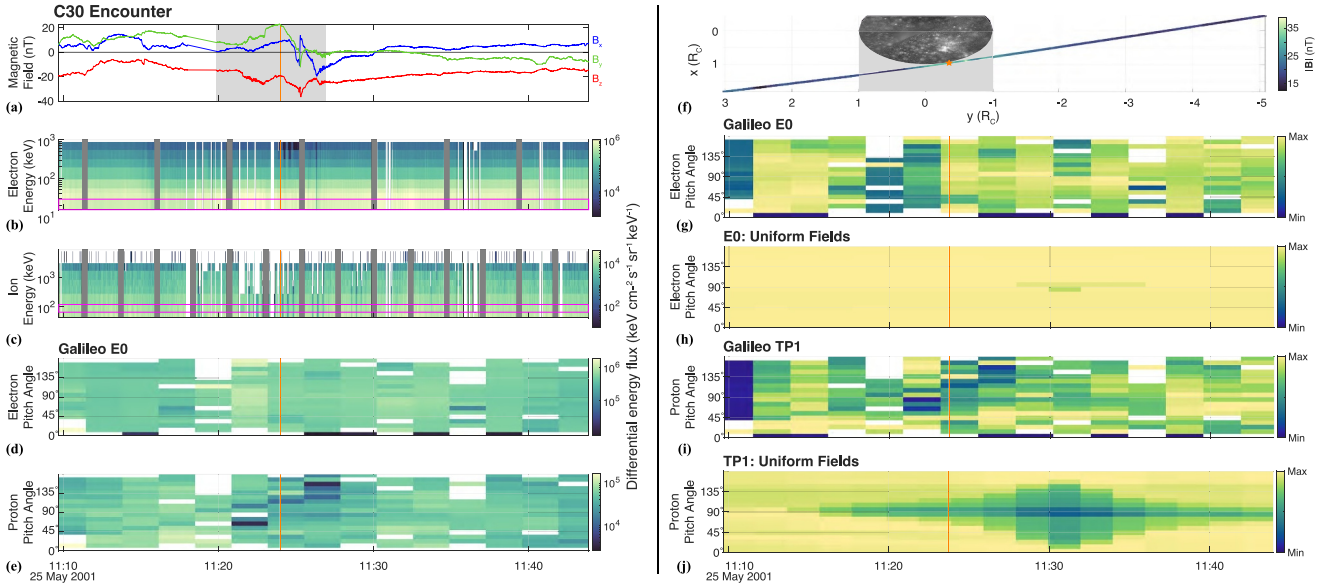

Figure 7. Magnetic field and energetic particle signatures during the C30 encounter of Callisto. The left column shows (a) magnetic field and (b–e) EPD observations, whereas the right column illustrates the (f) encounter trajectory colored to the magnetic field magnitude, (g, i) normalized PADs observed in the E0 and TP1 EPD channels, respectively, and (h, j) normalized PADs as modeled for these two channels using uniform fields near the moon. Dark gray vertical bars in panels (b, c) correspond to times when the EPD stepper motor was located at positions 0 (electrons and ions) and 7 (ions only). Note that since the direction of the C30 encounter was reversed compared to earlier flybys, the horizontal axis (showing the CphiO *y* coordinate) in panel (f) is reversed compared to previous figures.

electromagnetic environment in shaping the EPD signatures. Instead, to provide a first estimate for the effect that Callisto had on the observed energetic particle signatures, we trace energetic ions and electrons through uniform electromagnetic fields. We use a background magnetospheric field of $\mathbf{B}_0 = (5\hat{\mathbf{x}} + 0\hat{\mathbf{y}} - 12\hat{\mathbf{z}})$ nT obtained by extrapolating the field measured on both sides of Callisto to Galileo's closest approach, an ambient magnetospheric flow of $\mathbf{u}_0 = 192\hat{\mathbf{x}}$ km/s (consistent with, e.g., Kivelson et al., 2004), and the resulting convective electric field $\mathbf{E}_0 = -\mathbf{u}_0 \times \mathbf{B}_0$. Assuming the phase lag associated with Callisto's inductive response is near-zero (see, e.g., Kivelson et al., 1999; Zimmer et al., 2000), any induced field at Callisto during this encounter would have been weak, since the inducing components of the magnetospheric field are minimized at Jupiter's magnetic equator. Hence, we do not include the effect of an induced field on the EPD observations for this encounter.

Figures 7f–7j illustrate the results of this exercise in uniform fields. Figure 7h shows that Callisto's solid body does not strongly affect the modeled electron PADs along the C30 trajectory. However, the PAD of $E \approx 21$ keV electrons observed during the encounter (Figure 7g) is highly non-uniform with no systematic pattern discernible in the data, suggesting that the locally perturbed environment must have had a substantial effect on the electron PAD near the moon. Despite its low closest approach altitude, Figure 7h highlights that Galileo did not cross a *uniform* magnetic field line connected to Callisto's surface since there are no drop-outs at large pitch angles (but note that the magnetic field displayed strong deviations from uniform at these altitudes; see Figure 7a). For protons, the pitch angle distribution of the TP1 channel for the three bins near closest approach shows hints of a band of reduced flux that begins near pitch angles of $\alpha \approx 60°$ and extends to values of $\alpha \approx 140°$ approximately four minutes later, similar to the reductions visible in the proton channels during the C3 and C10 encounters. However, since C30 had the lowest closest approach altitude of the Callisto flybys, it is unclear why such a signature would be more restricted in pitch angle compared to the signatures detected during C3 and C10, and why it does not extend as far spatially along the C30 encounter's trajectory. Regardless, this signature is not consistent with the model for the case of uniform fields, which instead suggests a region of reduced flux near $\alpha \approx 90°$ that is present through most of the encounter. Near 11:30 UTC, this reduction expands to cover the range of pitch angles from $10° \lesssim \alpha \lesssim 160°$. The sense of gyration in a predominantly southward magnetospheric field causes protons in this hemisphere to gyrate into Callisto's surface before they are able to reach Galileo's position, generating the large-scale reduction. For electrons and ions alike, the poor pitch angle coverage of EPD caused many drop-outs in the PADs (see Figures 7d and 7e), making the features observed during C30 nearly impossible to interpret.

21699402, 2024, 2, Downloaded from https://agupubs.onlinelibrary.wiley.com/doi/10.1029/2023JA032189 by Univ of California Lawrence Berkeley National Lab, Wiley Online Library on [23/02/2024]. See the Terms and Conditions (https://onlinelibrary.wiley.com/terms-and-conditions) on Wiley Online Library for rules of use; OA articles are governed by the applicable Creative Commons License

21699402, 2024, 2, Downloaded from https://agupubs.onlinelibrary.wiley.com/doi/10.1029/2023JA032189 by Univ of California Lawrence Berkeley National Lab, Wiley Online Library on [23/02/2024]. See the Terms and Conditions (https://onlinelibrary.wiley.com/terms-and-conditions) on Wiley Online Library for rules of use; OA articles are governed by the applicable Creative Commons License

5. Conclusions

This study has presented energetic particle observations from four Galileo encounters of Callisto. By systematically comparing these observations to various model scenarios, we have investigated the role that the moon's perturbed electromagnetic environment—generated by a combination of its plasma interaction, induced field, and variability of the magnetospheric plasma—has on the energetic particle signatures detected by the EPD instrument.

We find that Galileo detected clear signatures of Callisto in the energetic particle pitch angle distributions during the spacecraft's close encounters. For energetic ions, since their gyroradii approach (and exceed) the size of Callisto, the moon's perturbed electromagnetic environment plays only a minor role in shaping their dynamics (see also Liuzzo et al., 2022). Instead, many observed features can be explained through geometric arguments: during three of the analyzed encounters (C3, C9, and C10), clear absorption signatures appeared in EPD ion observations due to particle shadowing by the moon's surface. EPD data from the C30 encounter is too sparse to provide an in-depth comparison, but our model results suggest that shadowing by Callisto's surface likely affected the precipitating energetic proton population during this encounter.

For energetic electrons, our results illustrate that Callisto's perturbed electromagnetic environment helped shape the signatures observed by EPD. Indeed, when considering the role of Callisto's induced field and plasma interaction on the electromagnetic field perturbations, we obtain a close match between numerous key features of the observed and modeled electron PADs. During C10, the moon's strong interaction with the low-energy magnetospheric plasma generated a region after closest approach wherein field-line draping dominated the magnetic field perturbations, causing EPD to detect a drop-out in the flux of electrons at near-perpendicular pitch angles. During C3, the moon's induced magnetic field helped to alter the ambient electron distribution, generating a flux bite-out at pitch angles of $\alpha \approx 90°$. For C9, the modeled flux reduction associated with electron dynamics in the perturbed electromagnetic environment is even narrower than the drop-out that was observed by Galileo, in that the modeled drop-out near pitch angles of $\alpha \approx 90°$ was detected for only a few minutes near closest approach. For each of the four encounters, our findings illustrate that it is not possible to understand the electron signatures observed by EPD when treating the magnetospheric fields near Callisto as uniform. In addition, our model results for each of the flybys do not indicate an electron population at field-aligned pitch angles, suggesting that the beamed electron distributions observed close to Callisto during the C3, C9, and C30 encounters may not be associated with the moon's local electromagnetic interaction.

Overall, our results highlight the important role that Callisto's induced field and plasma interaction have on energetic particle dynamics and point toward the importance of accurately representing the moon's local electromagnetic environment when analyzing energetic particle data. Our findings provide a critical context for measurements that will be obtained during the upcoming JUICE flybys of Callisto, providing a key piece of knowledge for understanding and identifying the moon's role in affecting its ambient energetic particle environment.

Appendix A: Averaging EPD Observations to Obtain Particle PADs

In EPD's high-gain antenna mode, the instrument motor stepped through 8 positions during the course of multiple spins of the spacecraft. In Figure A1, we include data from EPD over a ∼4 min period, illustrating the various positions of the (a) stepper motor and (b) spacecraft spin sectors, the (c) local pitch angle of EPD's look direction against $\mathbf{B}_0$, (d) differential electron energy flux in the E0 channel (center energy $E \approx 21$ keV), and (e) electron pitch angle in the E0 channel averaged over a full sweep of the stepper motor, binned into 10° increments. See Kollmann et al. (2022) for further details. The red and yellow shading in the figure correspond to the two time frames over which the data is averaged. As visible in Figure A1d, enhancements in the E0 differential electron energy flux were observed near 13:40:50 UTC, 13:43:14 UTC, and 13:43:45 UTC. These times correspond to look-directions near the maxima ($\alpha \approx 170°$), minima ($\alpha \approx 20°$), and maxima ($\alpha \approx 170°$) of pitch angle coverage, respectively (see orange coloring in Figure A1c). These enhancements are still visible in the electron pitch angles in channel E0 when averaging over the sweep of the EPD stepper motor (Figure A1e).

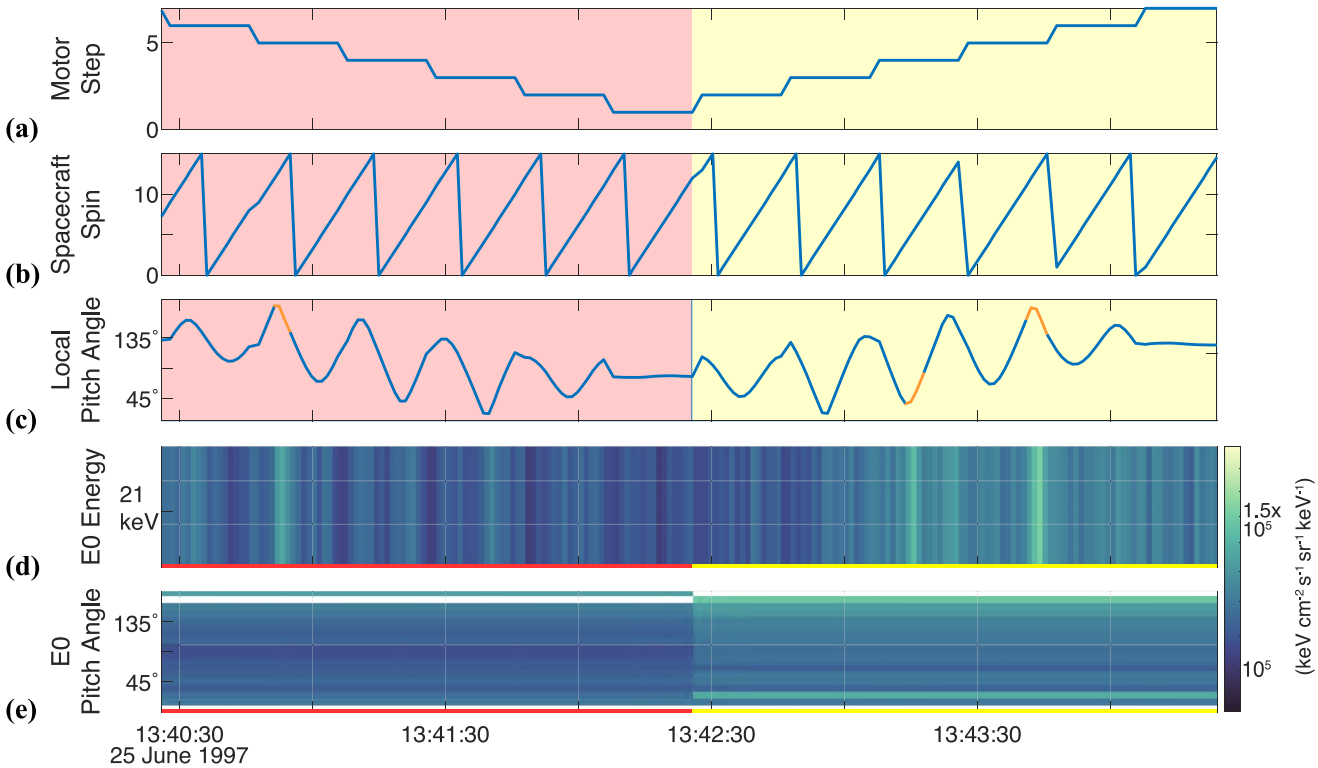

Figure A1. Sample data during consecutive sweeps of the EPD stepper motor. Red and yellow shading represents the time over which the observations are averaged to obtain energetic particle PADs. Orange coloring in the local pitch angle (panel c) corresponds to flux maxima detected in the E0 channel (panel d), which are still visible at the respective pitch angle after averaging (panel e).

Appendix B: Electron PADs in Uniform Plus Induced Dipole Fields

To isolate the role of Callisto's induced dipole on the electron PADs for encounters where the plasma interaction was weak, Figure B1 displays modeled electron PADs for the case of the superposition of Callisto's induced field with the Jovian magnetospheric background field during the (top) C3 and (bottom) C9 encounters. Hence, the perturbations do not consider any contribution from the moon's interaction with its ambient plasma environment,

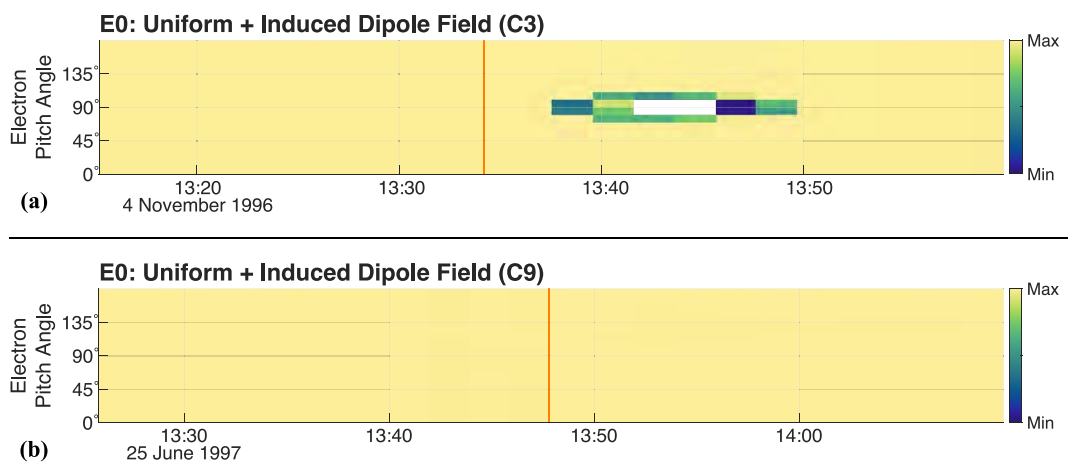

Figure B1. Normalized electron PADs during the (a) C3 and (b) C9 encounters, for the case of an induced dipolar field at Callisto superimposed with the uniform magnetospheric background field *without* any plasma interaction currents. See Figure 3 for further detail.

21699402, 2024, 2, Downloaded from https://agupubs.onlinelibrary.wiley.com/doi/10.1029/2023JA032189 by Univ of California Lawrence Berkeley National Lab, Wiley Online Library on [23/02/2024]. See the Terms and Conditions (https://onlinelibrary.wiley.com/terms-and-conditions) on Wiley Online Library for rules of use; OA articles are governed by the applicable Creative Commons License

21699402, 2024, 2, Downloaded from https://agupubs.onlinelibrary.wiley.com/doi/10.1029/2023JA032189 by Univ of California Lawrence Berkeley National Lab, Wiley Online Library on [23/02/2024]. See the Terms and Conditions (https://onlinelibrary.wiley.com/terms-and-conditions) on Wiley Online Library for rules of use; OA articles are governed by the applicable Creative Commons License

and the electromagnetic fields used for these scenarios do not require any results from the hybrid model since they can be expressed analytically (e.g., Liuzzo et al., 2015; Zimmer et al., 2000).

As visible in Figure B1, the pitch angle distribution of electrons in the Galileo E0 channel was not strongly affected by Callisto's plasma interaction during the C3 or the C9 encounters: compared to Figures 5d, 6d, B1a, and B1b are nearly identical. Since Callisto was located far from the center of the Jovian magnetospheric plasma sheet during these two flybys, the local magnetic field perturbations in B_x and B_y are well described by the superposition of an induced field with the magnetospheric background field (see, e.g., Kivelson et al., 1999; Liuzzo et al., 2015; Zimmer et al., 2000). For C3 in particular, the similarity between the electron PAD for the case of a uniform plus induced field (Figure B1a) and the distribution with the moon's weak plasma interaction included (Figure 5d) indicates that an Alfvén wing did not strongly contribute to the bite-out signature of $\alpha \approx 90°$ electrons observed in EPD after Galileo's closest approach (see further discussion in Section 4.2).

Data Availability Statement

Galileo EPD data are available in Kollmann (2022). Results from the AIKEF and GENTOo models are available at Liuzzo (2024).

Acknowledgments
The authors are supported by NASA Solar System Workings Grant 80NSSC21K0152. Resources supporting this work were provided by the NASA High-End Computing (HEC) Program through the NASA Advanced Supercomputing (NAS) Division at Ames Research Center.

References

Addison, P., Liuzzo, L., Arnold, H., & Simon, S. (2021). Influence of Europa's time-varying electromagnetic environment on magnetospheric ion precipitation and surface weathering. *Journal of Geophysical Research: Space Physics*, *126*(5), 1–42. https://doi.org/10.1029/2020JA029087

Carberry Mogan, S. R., Liuzzo, L., Poppe, A. R., Simon, S., Szalay, J. R., Tucker, O. J., & Johnson, R. E. (2023). Callisto's atmosphere: The oxygen enigma. *Journal of Geophysical Research: Planets*, *128*(9), 1–29. https://doi.org/10.1029/2023JE007894

Cochrane, C. J., Persinger, R. R., Vance, S. D., Midkiff, E. L., Castillo-Rogez, J., Luspay-Kuti, A., et al. (2022). Single- and multi-pass magnetometric subsurface ocean detection and characterization in icy worlds using principal component analysis (PCA): Application to triton. *Earth and Space Science*, *9*(2). https://doi.org/10.1029/2021EA002034

Compton, A. H., & Getting, I. A. (1935). An apparent effect of galactic rotation on the intensity of cosmic rays. *Physical Review*, *47*(11), 817–821. https://doi.org/10.1103/PhysRev.47.817

Divine, N., & Garrett, H. B. (1983). Charged particle distributions in Jupiter's magnetosphere. *Journal of Geophysical Research*, *88*(A9), 6889–6903. https://doi.org/10.1029/ja088ia09p06889

Galli, A., Vorburger, A., Carberry Mogan, S. R., Roussos, E., Stenberg Wieser, G., Wurz, P., et al. (2022). Callisto's atmosphere and its space environment: Prospects for the particle environment package on board JUICE. *Earth and Space Science*, *9*(5). https://doi.org/10.1029/2021EA002172

Gleeson, L. J., & Axford, W. I. (1968). The compton-getting effect. *Astrophysics and Space Science*, *2*(4), 431–437. https://doi.org/10.1007/BF02175919

Hartkorn, O., & Saur, J. (2017). Induction signals from Callisto's ionosphere and their implications on a possible subsurface ocean. *Journal of Geophysical Research: Space Physics*, *122*(11), 677–711. https://doi.org/10.1002/2017JA024269

Haynes, C., Tippens, T., Addison, P., Liuzzo, L., Poppe, A., & Simon, S. (2023). Emission of energetic neutral atoms from the magnetosphere-atmosphere interactions at Callisto and Europa. *Journal of Geophysical Research: Space Phusics*, *128*(10), e2023JA031931. https://doi.org/10.1029/2023JA031931

Hendrix, A. R., & Johnson, R. E. (2008). Callisto: New insights from Galileo disk-resolved UV measurements. *The Astrophysical Journal*, *687*(1), 706–713. https://doi.org/10.1086/591491

Hess, S. L. G. L. G., Delamere, P. A. A., Dols, V., & Ray, L. C. C. (2011). Comparative study of the power transferred from satellite-magnetosphere interactions to auroral emissions. *Journal of Geophysical Research*, *116*(1), A01202. https://doi.org/10.1029/2010JA015807

Huybrighs, H. L., Blöcker, A., Roussos, E., van Buchem, C., Futaana, Y., Holmberg, M. K., et al. (2023). Europa's perturbed fields and induced dipole affect energetic proton depletions during distant Alfvén wing flybys. *Journal of Geophysical Research: Space Physics*, *128*(9), 1–37. https://doi.org/10.1029/2023JA031420

Huybrighs, H. L., Roussos, E., Blöcker, A., Krupp, N., Futaana, Y., Barabash, S., et al. (2020). An active plume eruption on Europa during Galileo Flyby E26 as indicated by energetic proton depletions. *Geophysical Research Letters*, *47*(10), e2020GL087806. https://doi.org/10.1029/2020GL087806

Jacobsen, S., Saur, J., Neubauer, F. M., Bonfond, B., Gérard, J., & Grodent, D. (2010). Location and spatial shape of electron beams in Io's wake. *Journal of Geophysical Research*, *115*(A4), A04205. https://doi.org/10.1029/2009ja014753

Jia, X., Kivelson, M. G., & Paranicas, C. (2021). Comment on "an active plume eruption on Europa during Galileo Flyby E26 as indicated by energetic proton depletions" by Huybrighs et al. *Geophysical Research Letters*, *48*(6), 1–4. https://doi.org/10.1029/2020GL091550

Khurana, K. K. (1997). Euler potential models of Jupiter's magnetospheric field. *Journal of Geophysical Research*, *102*(A6), 11295–11306. https://doi.org/10.1029/97JA00563

Khurana, K. K., Kivelson, M. G., Stevenson, D. J., Schubert, G., Russell, C. T., Walker, R. J., & Polanskey, C. (1998). Induced magnetic fields as evidence for subsurface oceans in Europa and Callisto. *Nature*, *395*(6704), 777–780. https://doi.org/10.1038/27394

Khurana, K. K., & Schwarzl, H. K. (2005). Global structure of Jupiter's magnetospheric current sheet. *Journal of Geophysical Research*, *110*(A7). https://doi.org/10.1029/2004JA010757

Kivelson, M., Bagenal, F., Kurth, W., Neubauer, F., Paranicas, C., & Saur, J. (2004). Magnetospheric interactions with satellites. In *Jupiter: The planet, satellites and magnetosphere* (pp. 513–536).

Kivelson, M., Khurana, K., Stevenson, D., Bennett, L., Joy, S., Russell, C., et al. (1999). Europa and Callisto: Induced or intrinsic fields in a periodically varying plasma environment. *Journal of Geophysical Research*, *104*, 4609. https://doi.org/10.1029/1998JA900095

Kliore, A. J. J., Anabtawi, A., Herrera, R. G. G., Asmar, S. W. W., Nagy, A. F. F., Hinson, D. P. P., & Flasar, F. M. M. (2002). Ionosphere of Callisto from Galileo radio occultation observations. *Journal of Geophysical Research*, *107*(May), 1–7. https://doi.org/10.1029/2002JA009365

Knight, S. (1973). Parallel electric fields. *Planetary and Space Science*, *21*(5), 741–750. https://doi.org/10.1016/0032-0633(73)90093-7
Kollmann, P. (2022). Galileo EPD calibrated corrected data bundle. https://doi.org/10.17189/n0dm-0014
Kollmann, P., Clark, G., Paranicas, C., Mauk, B., Haggerty, D., Rymer, A., & Allegrini, F. (2022). Ganymede's radiation cavity and radiation belts. *Geophysical Research Letters*, *49*(23), 1–10. https://doi.org/10.1029/2022GL098474
Krupp, N., Kotova, A., Roussos, E., Simon, S., Liuzzo, L., Paranicas, C., et al. (2020). Magnetospheric interactions of Saturn's Moon Dione (2005–2015). *Journal of Geophysical Research: Space Physics*, *125*(6). https://doi.org/10.1029/2019JA027688
Krupp, N., Roussos, E., Fränz, M., Kollmann, P., Paranicas, C., Clark, G., et al. (2023). Pitch angle distributions of energetic particles near Callisto. *Journal of Geophysical Research: Space Physics*, *128*(10), 1–13. https://doi.org/10.1029/2023JA031794
Krupp, N., Vasyliunas, V. M., Woch, J., Lagg, A., & Sonnensystemforschung, M.-p.-i. (2004). Dynamics of the Jovian magnetosphere. In F. Bagenal, T. Dowling, & W. McKinnon (Eds.), *Jupiter: The planet, satellites and magnetosphere (chap. 25)*. Cambridge University Press.
Lee-Payne, Z., Kollmann, P., Grande, M., & Knight, T. (2020). Correction of Galileo energetic particle detector, composition measurement system high rate data: Semiconductor dead layer correction. *Space Science Reviews*, *216*(1), 5. https://doi.org/10.1007/s11214-019-0621-y
Lindkvist, J., Holmström, M., Khurana, K. K., Fatemi, S., & Barabash, S. (2015). Callisto plasma interactions: Hybrid modeling including induction by a subsurface ocean. *Journal of Geophysical Research: Space Physics*, *120*(6), 4877–4889. https://doi.org/10.1002/2015JA021212
Liuzzo, L. (2024). Data for "Constraining the influence of Callisto's perturbed electromagnetic environment on energetic particle observations" by Liuzzo et al. (2024). https://doi.org/10.5281/zenodo.10475527
Liuzzo, L., Feyerabend, M., Simon, S., & Motschmann, U. (2015). The impact of Callisto's atmosphere on its plasma interaction with the Jovian magnetosphere. *Journal of Geophysical Research: Space Physics*, *120*(11), 9401–9427. https://doi.org/10.1002/2015JA021792
Liuzzo, L., Poppe, A. R., Addison, P., Simon, S., Nénon, Q., & Paranicas, C. (2022). Energetic magnetospheric particle fluxes onto Callisto's atmosphere. *Journal of Geophysical Research: Space Physics*, *127*(11), 1–30. https://doi.org/10.1029/2022JA030915
Liuzzo, L., Simon, S., & Feyerabend, M. (2018). Observability of Callisto's inductive signature during the JUpiter ICy Moons Explorer mission. *Journal of Geophysical Research: Space Physics*, *123*(11), 9045–9054. https://doi.org/10.1029/2018JA025951
Liuzzo, L., Simon, S., Feyerabend, M., & Motschmann, U. (2016). Disentangling plasma interaction and induction signatures at Callisto: The Galileo C10 flyby. *Journal of Geophysical Research: Space Physics*, *121*(9), 8677–8694. https://doi.org/10.1002/2016JA023236
Liuzzo, L., Simon, S., Feyerabend, M., & Motschmann, U. (2017). Magnetic signatures of plasma interaction and induction at Callisto: The Galileo C21, C22, C23, and C30 flybys. *Journal of Geophysical Research: Space Physics*, *122*(7), 7364–7386. https://doi.org/10.1002/2017JA024303
Liuzzo, L., Simon, S., & Regoli, L. (2019a). Energetic electron dynamics near Callisto. *Planetary and Space Science*, *179*(August), 104726. https://doi.org/10.1016/j.pss.2019.104726
Liuzzo, L., Simon, S., & Regoli, L. (2019b). Energetic ion dynamics near Callisto. *Planetary and Space Science*, *166*, 23–53. https://doi.org/10.1016/j.pss.2018.07.014
Mauk, B. H., Mitchell, D. G., McEntire, R. W., Paranicas, C. P., Roelof, E. C., Williams, D. J., et al. (2004). Energetic ion characteristics and neutral gas interactions in Jupiter's magnetosphere. *Journal of Geophysical Research*, *109*(A9), A09S12. https://doi.org/10.1029/2003JA010270
Mauk, B. H., & Saur, J. (2007). Equatorial electron beams and auroral structuring at Jupiter. *Journal of Geophysical Research*, *112*(A10), A10221. https://doi.org/10.1029/2007JA012370
Müller, J., Simon, S., Motschmann, U., Schüle, J., Glassmeier, K. H., & Pringle, G. J. (2011). A.I.K.E.F.: Adaptive hybrid model for space plasma simulations. *Computer Physics Communications*, *182*(4), 946–966. https://doi.org/10.1016/j.cpc.2010.12.033
Nénon, Q. (2022). Galileo-EPD electron PADs. https://doi.org/10.6084/m9.figshare.20180222.v1
Nénon, Q., Miller, L. P., Kollmann, P., Liuzzo, L., Pinto, M., & Witasse, O. (2022). Pitch angle distribution of MeV electrons in the magnetosphere of Jupiter. *Journal of Geophysical Research: Space Physics*, *127*(8), 1–21. https://doi.org/10.1029/2022JA030627
Neubauer, F. (1999). Alfvén wings and electromagnetic induction in the interiors: Europa and Callisto. *Journal of Geophysical Research*, *104*(A12), 28671–28684. https://doi.org/10.1029/1999JA900217
Paranicas, C., Hibbitts, C. A., Kollmann, P., Ligier, N., Hendrix, A. R., Nordheim, T. A., et al. (2018). Magnetospheric considerations for solar system ice state. *Icarus*, *302*, 560–564. https://doi.org/10.1016/j.icarus.2017.12.013
Poppe, A. R., Fatemi, S., & Khurana, K. K. (2018). Thermal and energetic ion dynamics in Ganymede's magnetosphere. *Journal of Geophysical Research: Space Physics*, *123*(6), 4614–4637. https://doi.org/10.1029/2018JA025312
Rabia, J., Hue, V., Szalay, J. R., André, N., Nénon, Q., Blanc, M., et al. (2023). Evidence for non-monotonic and broadband electron distributions in the Europa footprint tail revealed by Juno in situ measurements. *Geophysical Research Letters*, *50*(12), 1–9. https://doi.org/10.1029/2023gl103131
Roussos, E., Kollmann, P., Krupp, N., Paranicas, C., Krimigis, S. M., Mitchell, D. G., et al. (2012). Energetic electron observations of Rhea's magnetospheric interaction. *Icarus*, *221*(1), 116–134. https://doi.org/10.1016/j.icarus.2012.07.006
Santolík, O., Gurnett, D. A. A., Jones, G. H. H., Schippers, P., Crary, F. J. J., Leisner, J. S. S., et al. (2011). Intense plasma wave emissions associated with Saturn's moon Rhea. *Geophysical Research Letters*, *38*(19), L19204. https://doi.org/10.1029/2011GL049219
Saur, J., Neubauer, F. M., & Glassmeier, K.-H. H. (2010). Induced magnetic fields in solar system bodies. *Space Science Reviews*, *152*(1–4), 391–421. https://doi.org/10.1007/s11214-009-9581-y
Selesnick, R. S., & Cohen, C. M. S. (2009). Charge states of energetic ions in Jupiter's radiation belt inferred from absorption microsignatures of Io. *Journal of Geophysical Research*, *114*(A1), A01207. https://doi.org/10.1029/2008JA013722
Seufert, M. (2012). Callisto: Induction signals, atmosphere and plasma interaction (Unpublished doctoral dissertation). Universität zu Köln.
Szalay, J. R., Allegrini, F., Bagenal, F., Bolton, S. J., Bonfond, B., Clark, G., et al. (2020). A New framework to explain changes in Io's footprint tail electron fluxes. *Geophysical Research Letters*, *47*(18). https://doi.org/10.1029/2020GL089267
USGS. (2002). Controlled photomosaic map of Callisto JC 15M CMN (Tech. Rep.). https://doi.org/10.3133/i2770
Vance, S. D., Styczinski, M. J., Bills, B. G., Cochrane, C. J., Soderlund, K. M., Gómez-Pérez, N., & Paty, C. (2021). Magnetic induction responses of Jupiter's ocean moons including effects from adiabatic convection. *Journal of Geophysical Research: Planets*, *126*(2), 1–25. https://doi.org/10.1029/2020JE006418
Williams, D. J., McEntire, R. W., Jaskulek, S., & Wilken, B. (1992a). The Galileo energetic particles detector. *Space Science Reviews*, *60*(1–4), 385–412. https://doi.org/10.1007/BF00216863
Williams, D. J., McEntire, R. W., Jaskulek, S., & Wilken, B. (1992b). The Galileo energetic particles detector. *Space Science Reviews*, *60*(1–4), 385–412. https://doi.org/10.1007/BF00216863
Zimmer, C., Khurana, K. K., & Kivelson, M. G. (2000). Subsurface oceans on Europa and Callisto: Constraints from Galileo magnetometer observations. *Icarus*, *347*(2), 329–347. https://doi.org/10.1006/icar.2000.6456

21699402, 2024, 2, Downloaded from https://agupubs.onlinelibrary.wiley.com/doi/10.1029/2023JA032189 by Univ of California Lawrence Berkeley National Lab, Wiley Online Library on [23/02/2024]. See the Terms and Conditions (https://onlinelibrary.wiley.com/terms-and-conditions) on Wiley Online Library for rules of use; OA articles are governed by the applicable Creative Commons License